ELECTRONIC SUPPLEMENTARY INFORMATION

for

Coupling Between two Ru(bda) Catalysts Bridged by a *trans*-dicyano Complex

Pedro O. Abate,[a,b] Virginia M. Juárez,[a,b] and Luis M. Baraldo[a,b]

[a] Universidad de Buenos Aires, Facultad de Ciencias Exactas y Naturales, Departamento de Química Inorgánica, Analítica y Química Física, Pabellón 2, Ciudad Universitaria, C1428EHA, Buenos Aires, Argentina.
[b] CONICET – Universidad de Buenos Aires. Instituto de Química Física de Materiales, Medio Ambiente y Energía (INQUIMAE), Pabellón 2, Ciudad Universitaria, C1428EHA, Buenos Aires, Argentina.

Table of contents

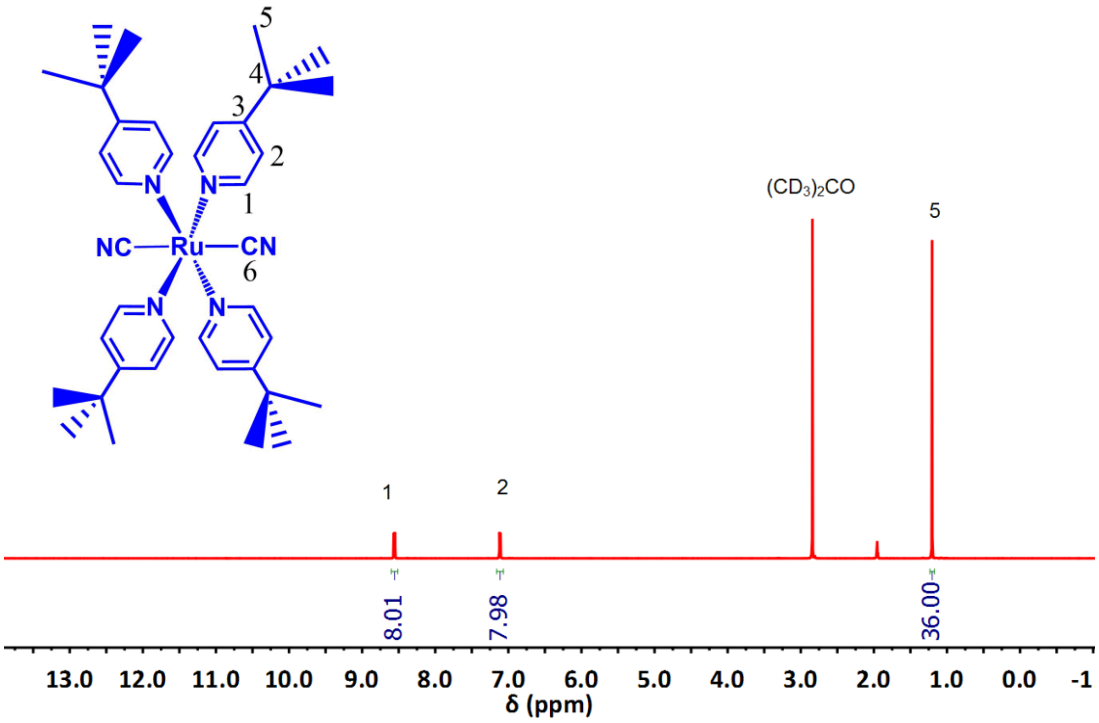

Fig. S1 500 MHz ^{1}H-NMR spectrum of ***trans*-Ru(tbupy)$_4$(CN)$_2$** dissolved in $(CD_3)_2CO$.

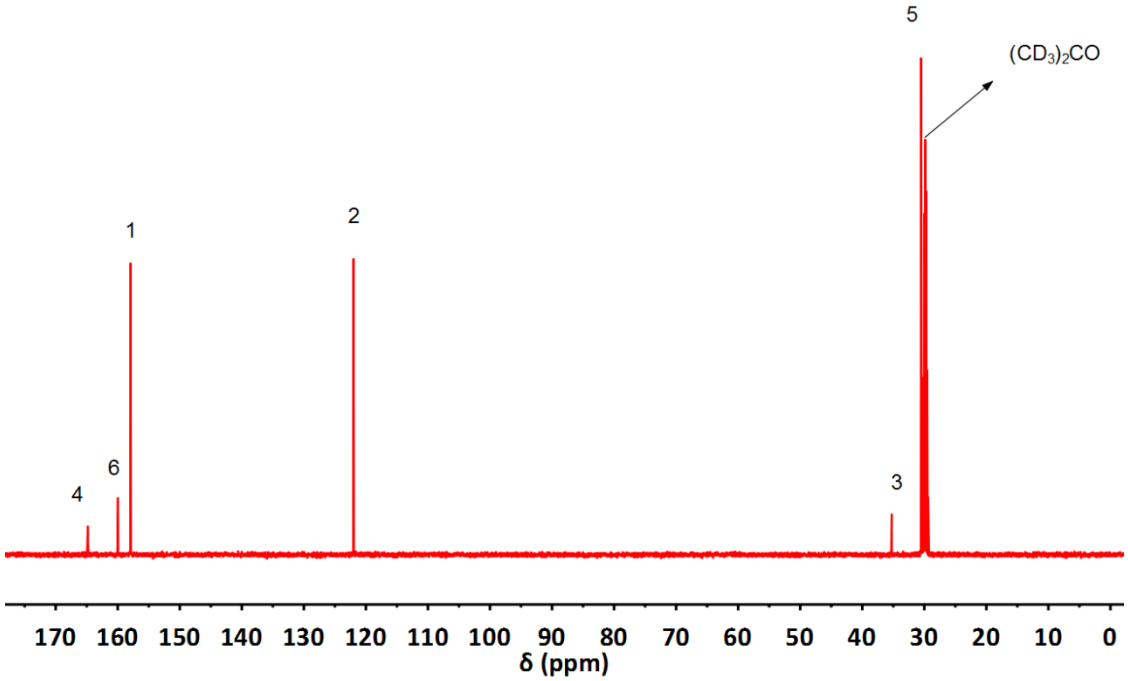

Fig. S2 125 MHz ^{13}C-NMR spectrum of ***trans*-Ru(tbupy)$_4$(CN)$_2$** dissolved in $(CD_3)_2CO$.

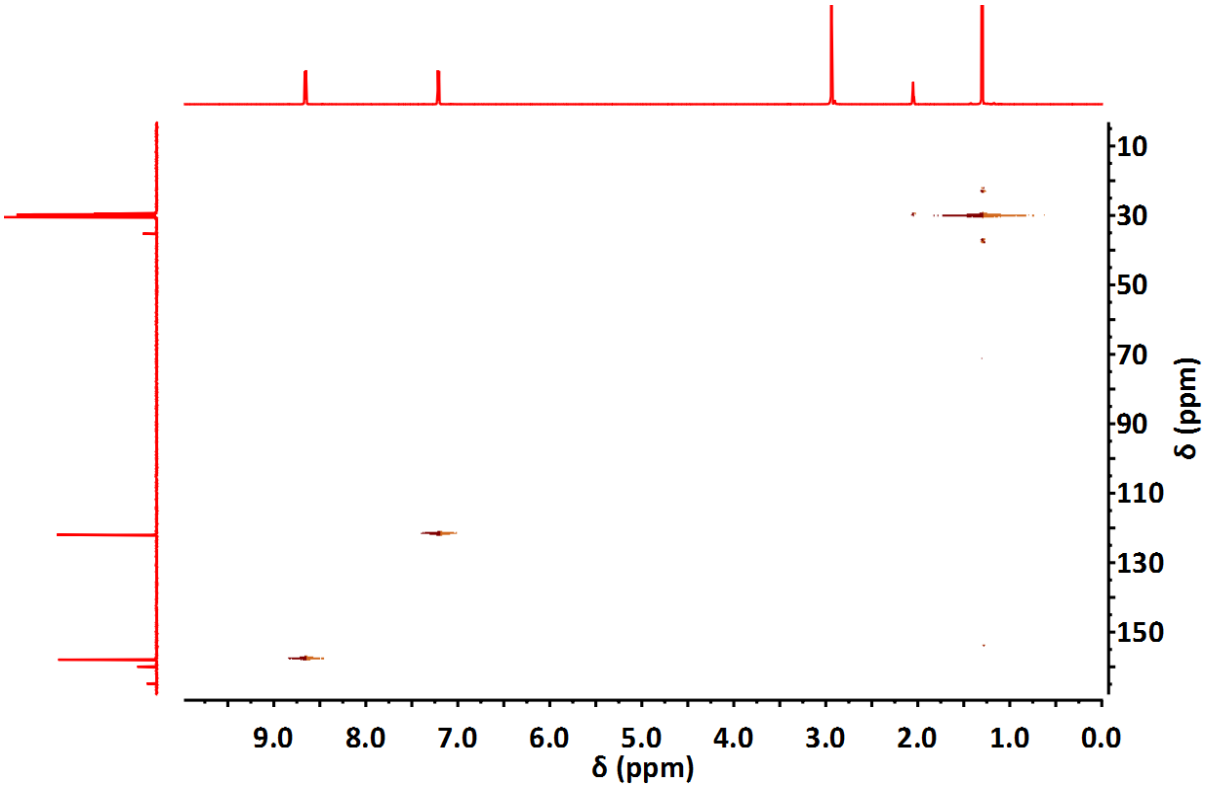

Fig. S3 2D ^{1}H-^{13}C HSQC spectrum of ***trans*-Ru(tbupy)$_4$(CN)$_2$** dissolved in $(CD_3)_2CO$.

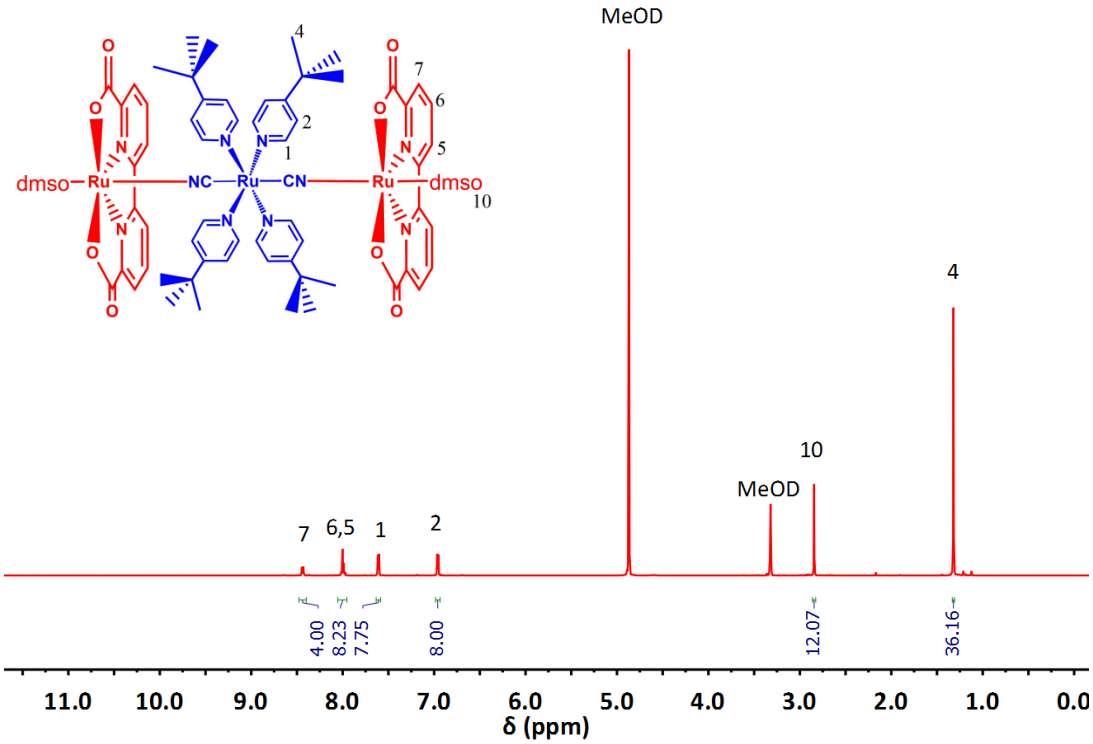

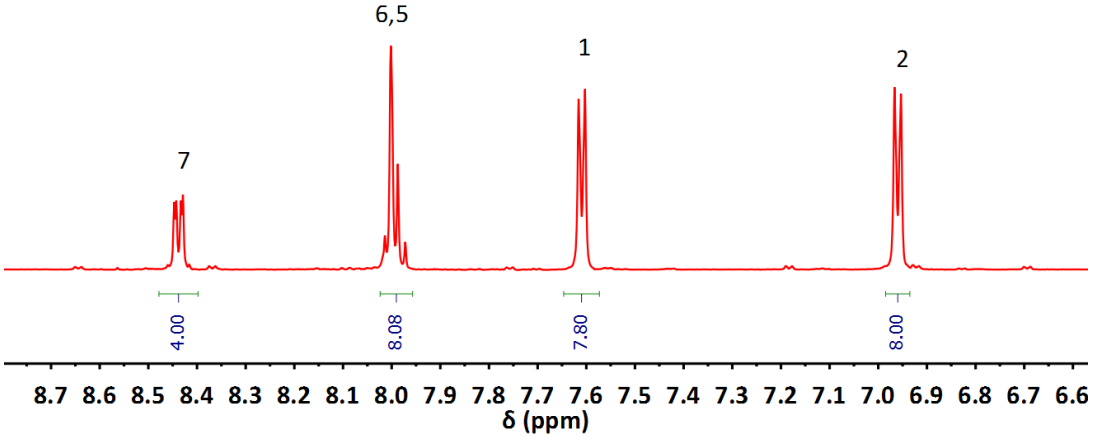

Fig. S4 500 MHz ^{1}H-NMR spectrum of **[RuRu(tbupy)$_4$Ru]** dissolved in CD_3OD.

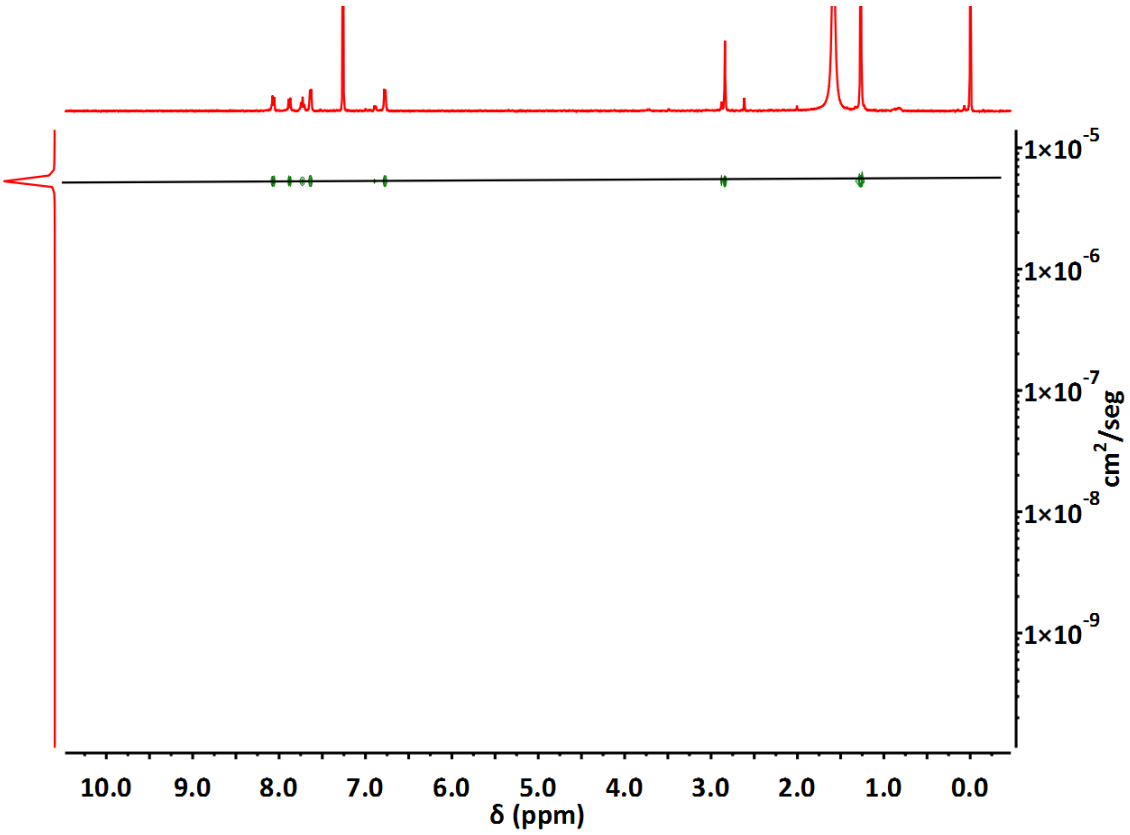

Fig. S5 ^{1}H-DOSY spectrum of **[RuRu(tbupy)$_4$Ru]** in $CDCl_3$ at 298K. The diffusion coefficient is $5.31*10^{-6}$ cm^2/s.

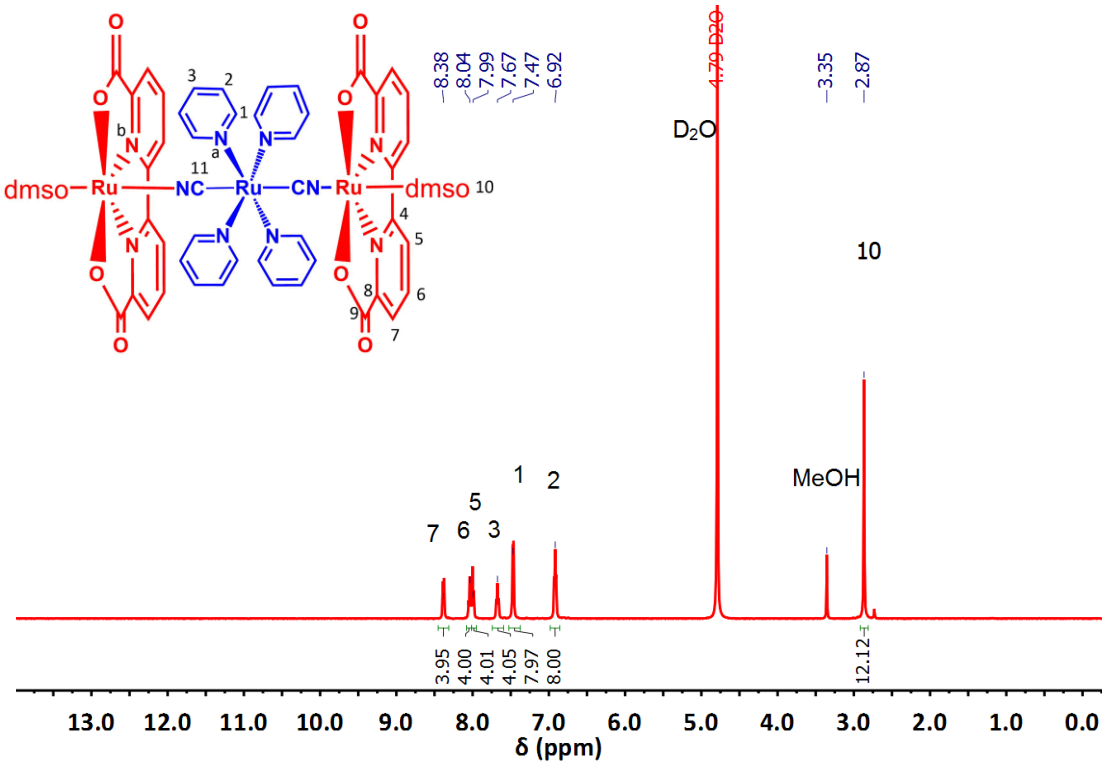

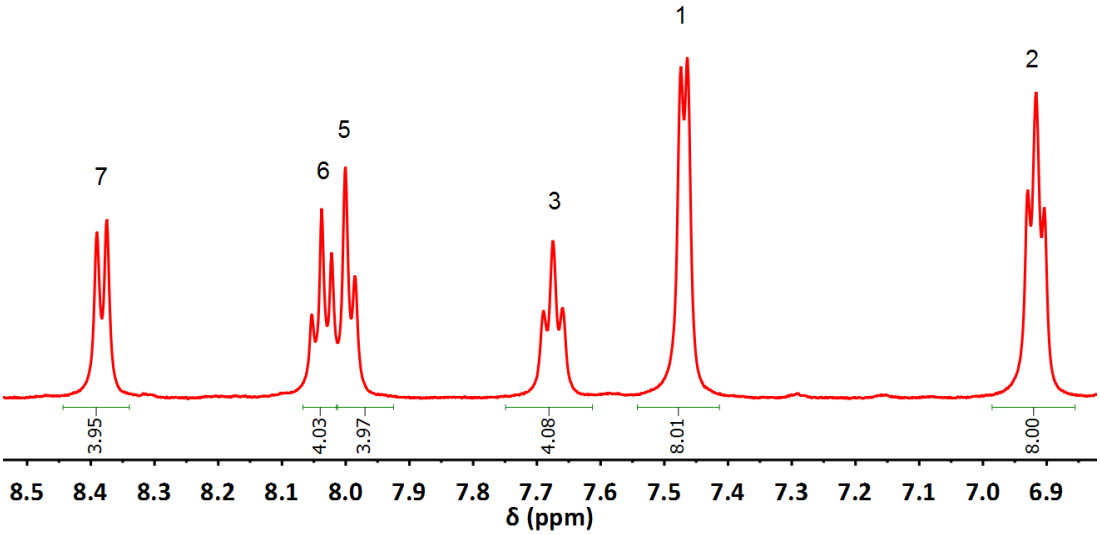

Fig. S6 500 MHz ^{1}H-NMR spectrum of **[RuRu(py)$_4$Ru]** dissolved in D_2O.

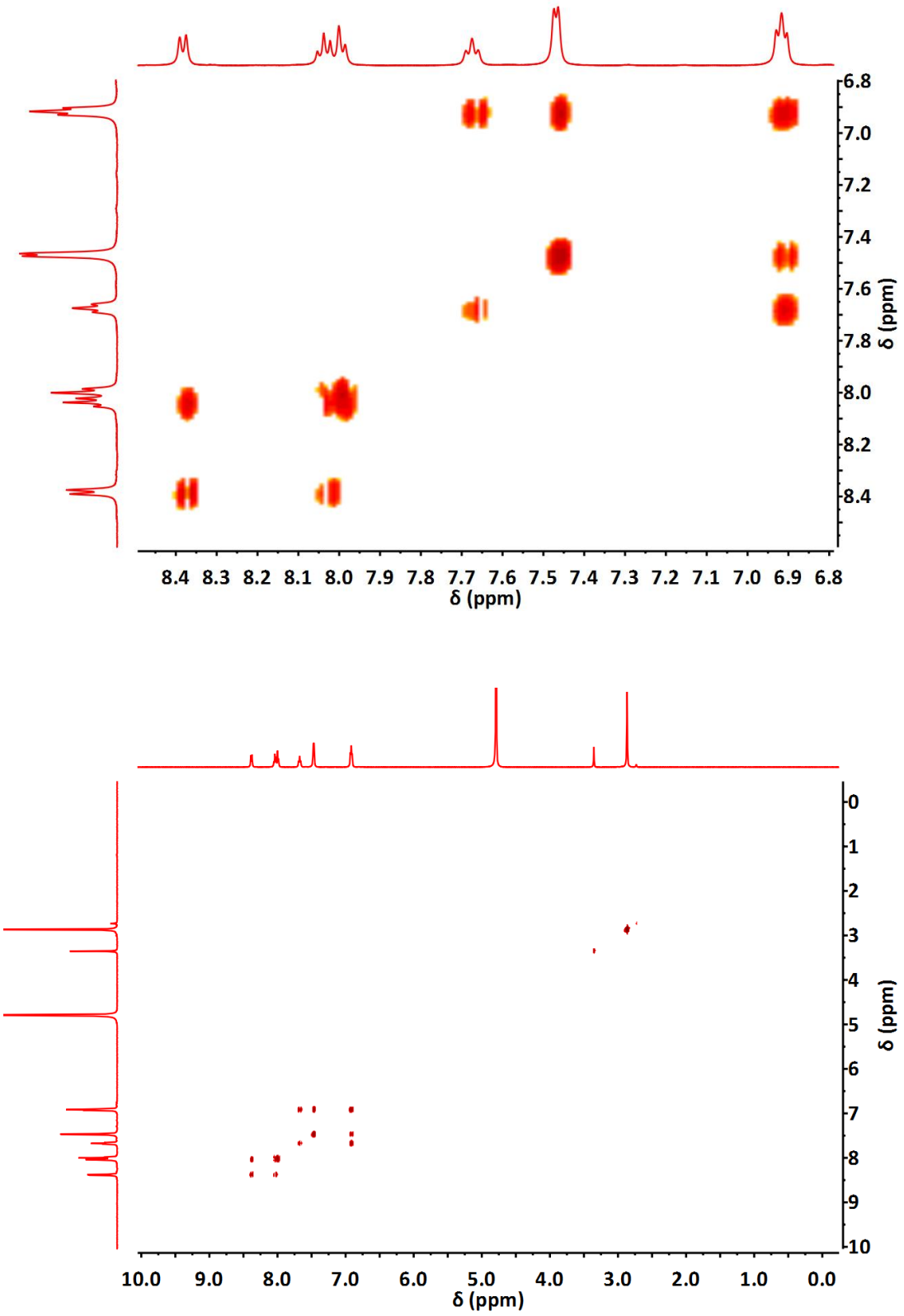

Fig. S7 2D ^{1}H-^{1}H COSY spectrum of **[RuRu(py)$_4$Ru]** dissolved in D_2O.

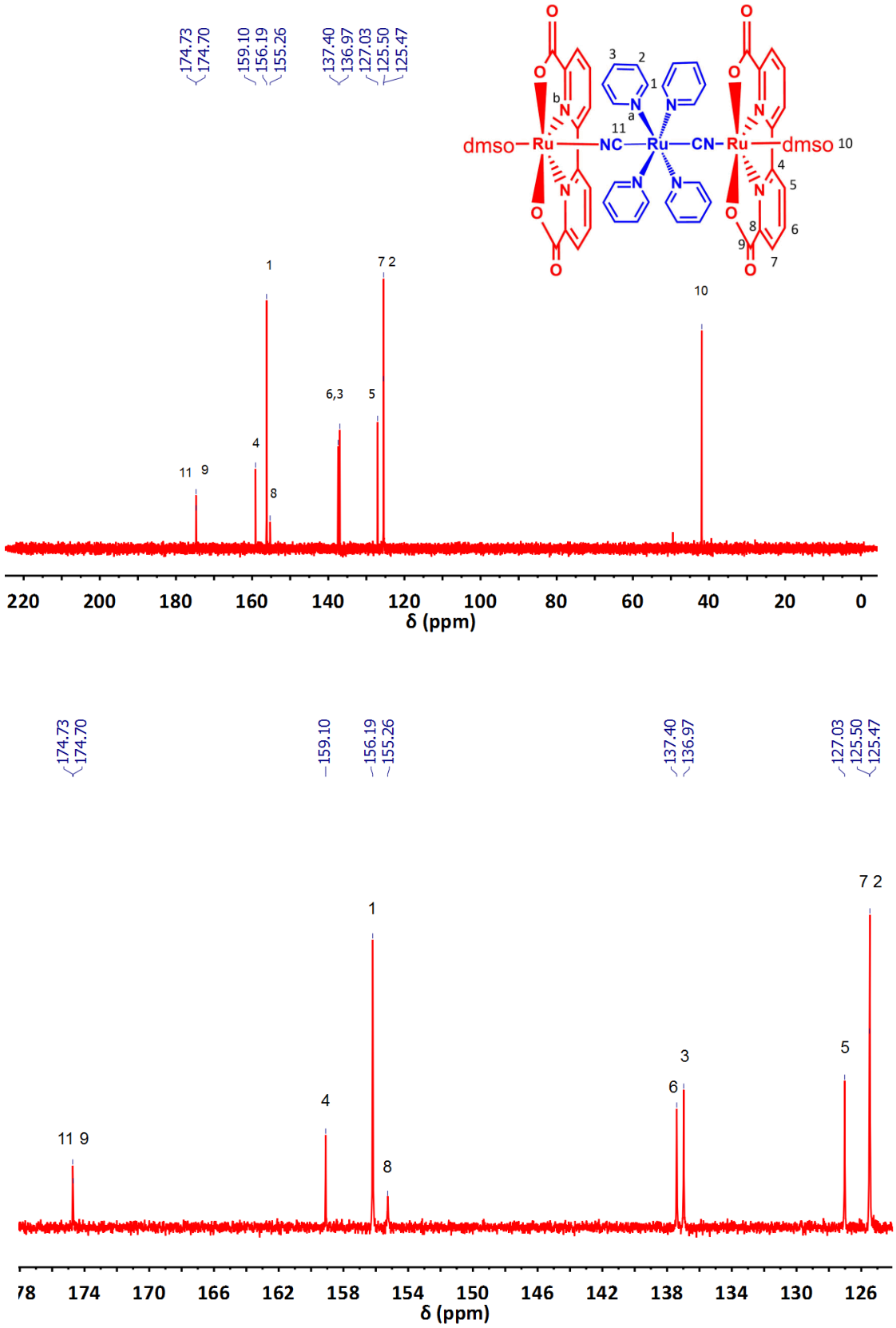

Fig. S8 125 MHz ^{13}C-NMR spectrum of **[RuRu(py)$_4$Ru]** dissolved in D_2O.

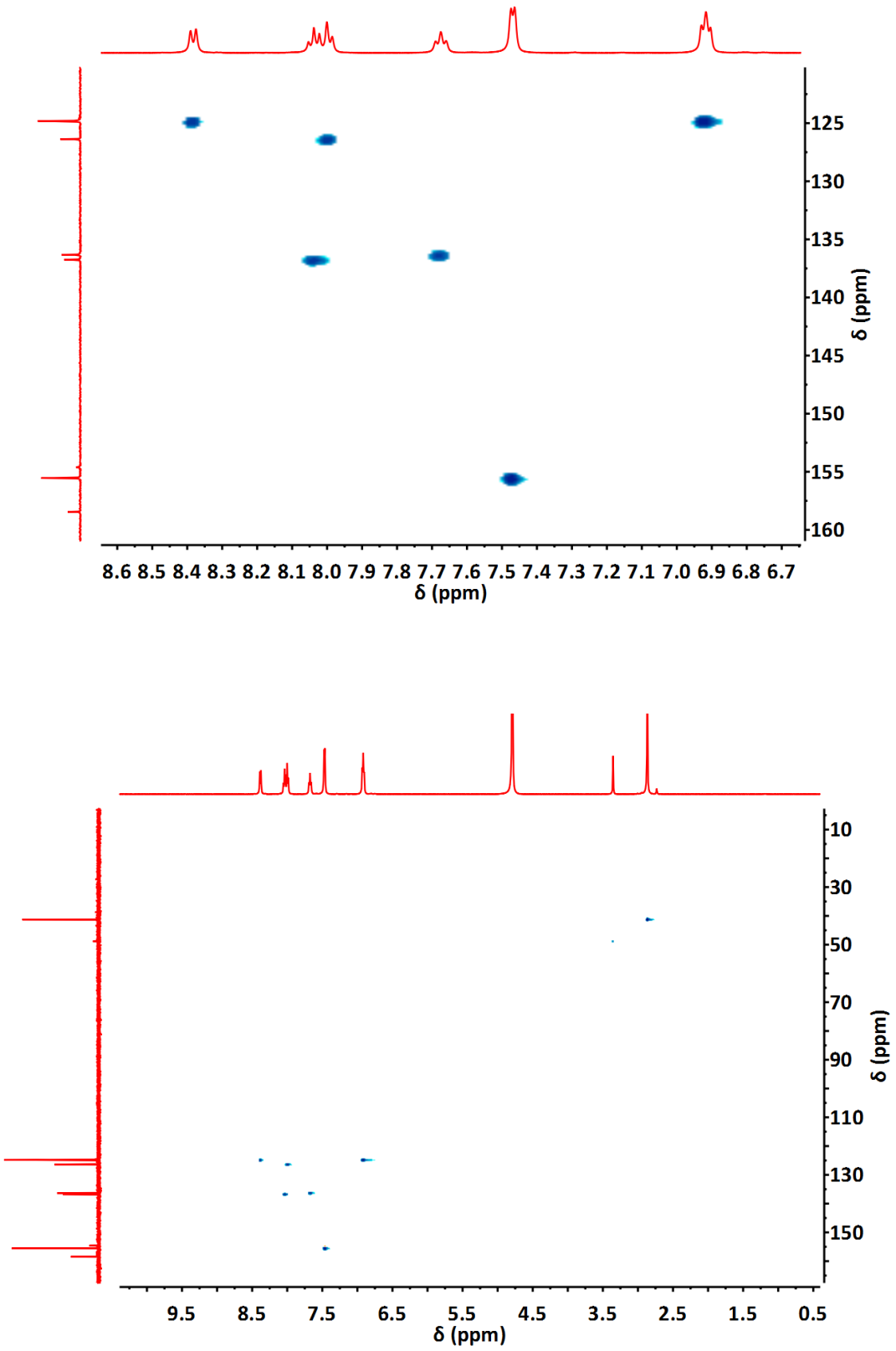

Fig. S9 2D ^{1}H-^{13}C HSQC spectrum of **[RuRu(py)$_4$Ru]** dissolved in D_2O.

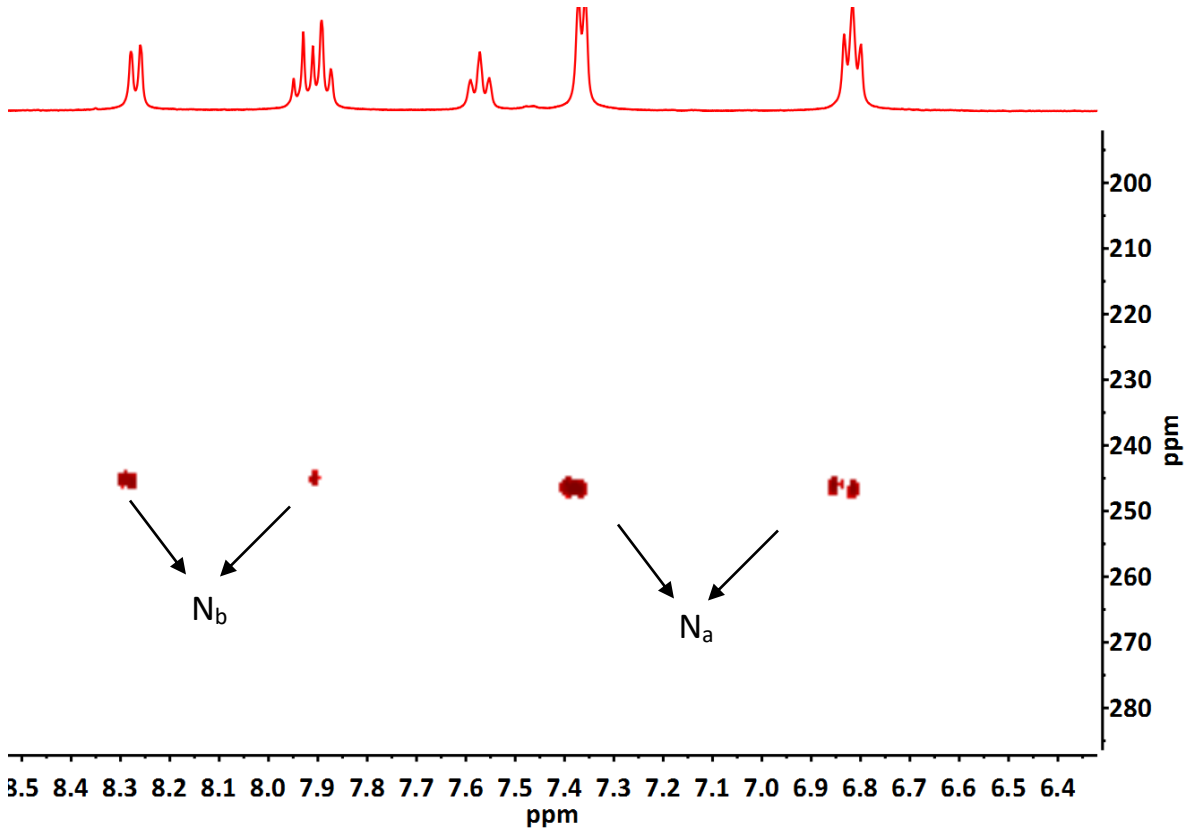

Fig. S10 2D ^{1}H-^{15}N HSQC spectrum of **[RuRu(py)$_4$Ru]** dissolved in D_2O.

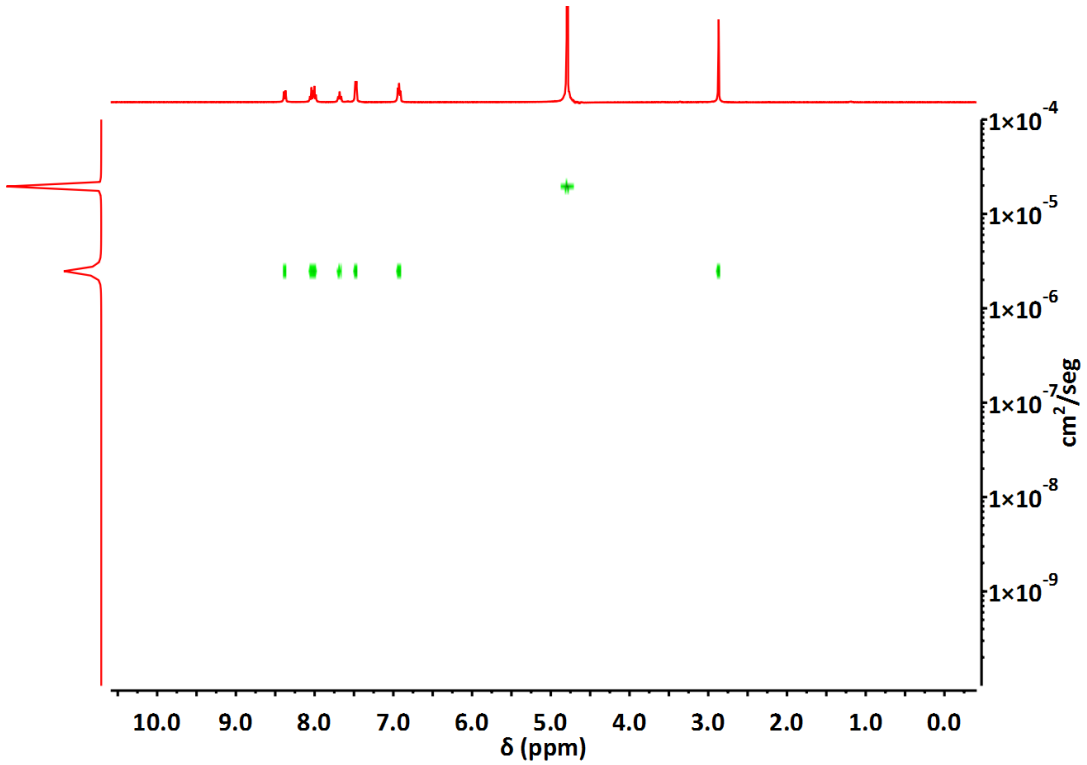

Fig. S11 ^{1}H-DOSY spectrum of **[RuRu(py)$_4$Ru]** in D_2O at 298K. The diffusion coefficient is $2.48*10^{-6}$ cm^2/s.

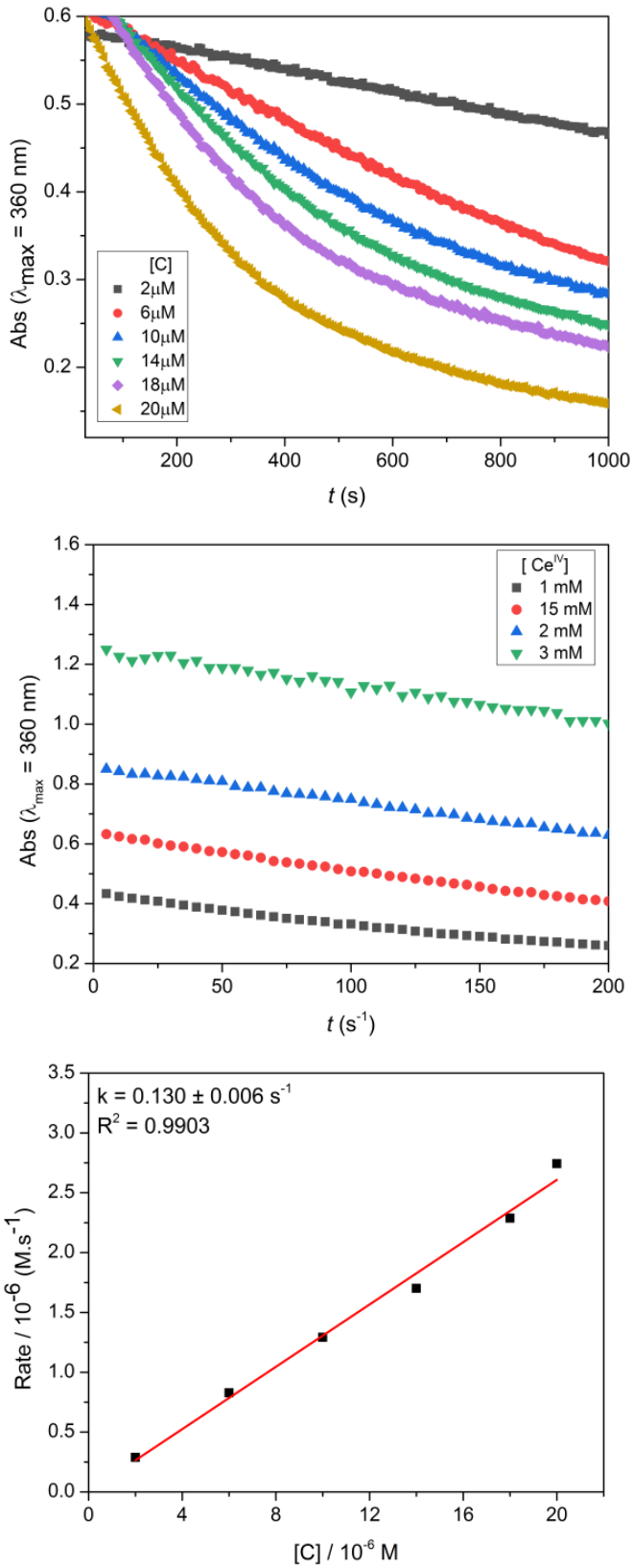

Fig. S12 Absorbance decay monitored at 360 nm in aqueous solution as a function of time for different **[RuRu(py)$_4$Ru]** concentrations (top) and for different Ce(IV) concentrations (center). Plot of the rate constant *vs* **[RuRu(py)$_4$Ru]** concentrations (bottom). Conditions: pH = 1.0 (aqueous 0.1 M triflic acid) and *T* = 298 K.

Calculation of the number of transferred electrons

Fig. S13 shows the fit of the plot of i_p vs the $v^{1/2}$ used for the calculation of the number of transferred electrons according with the Randles-Ševčík equation (1) where i_p is the anodic peak current α, n is the number of transferred electrons, F is the Faraday constant (96500 C), A is the active area of the working electrode (0.0707 cm^2), C is the catalyst concentration in mol cm^{-3}, v is the scan rate in V s^{-1}, D is the diffusion coefficient (cm^2 s^{-1}) calculated from ^{1}H-DOSY experiments, T is the temperature in kelvin and R is the ideal gas constant (8.314 J mol^{-1} K^{-1}).

$$i_p = 0.4463nFAC\left(\frac{nFvD}{RT}\right)^{\frac{1}{2}} \qquad (1)$$

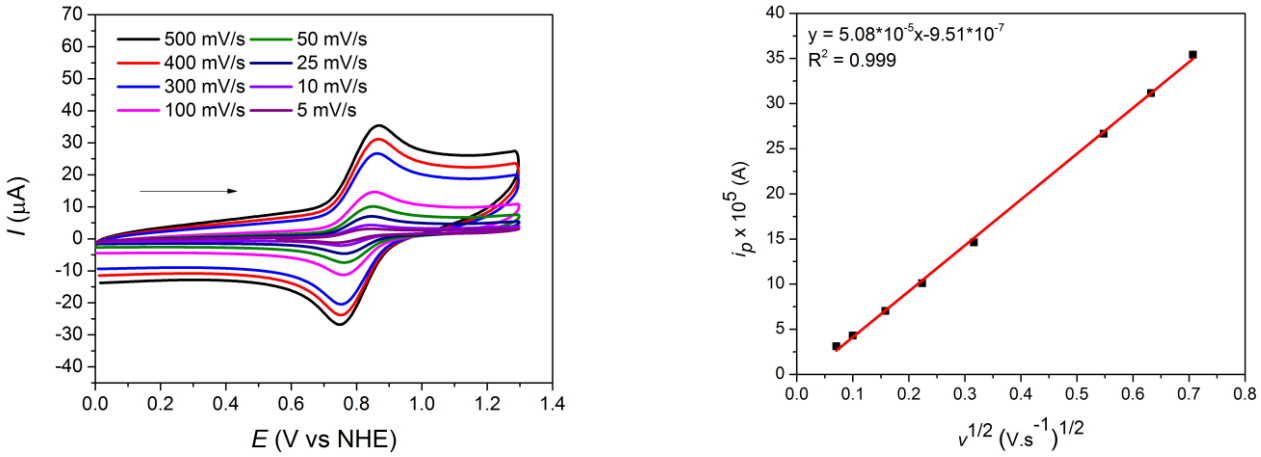

Fig. S13 Left: CV of **[RuRu(tbupy)$_4$Ru]** in CH_2Cl_2 (0.2 M $TBAPF_6$) at different scan rates. Right: plot of the anodic current i_p ($Ru^{III/II}$) *vs* square root of the scan rate ($v^{1/2}$). Conditions: WE (glassy carbon electrode), CE (platinum wire), RE (Ag wire) and [C] = 0.41 mM.

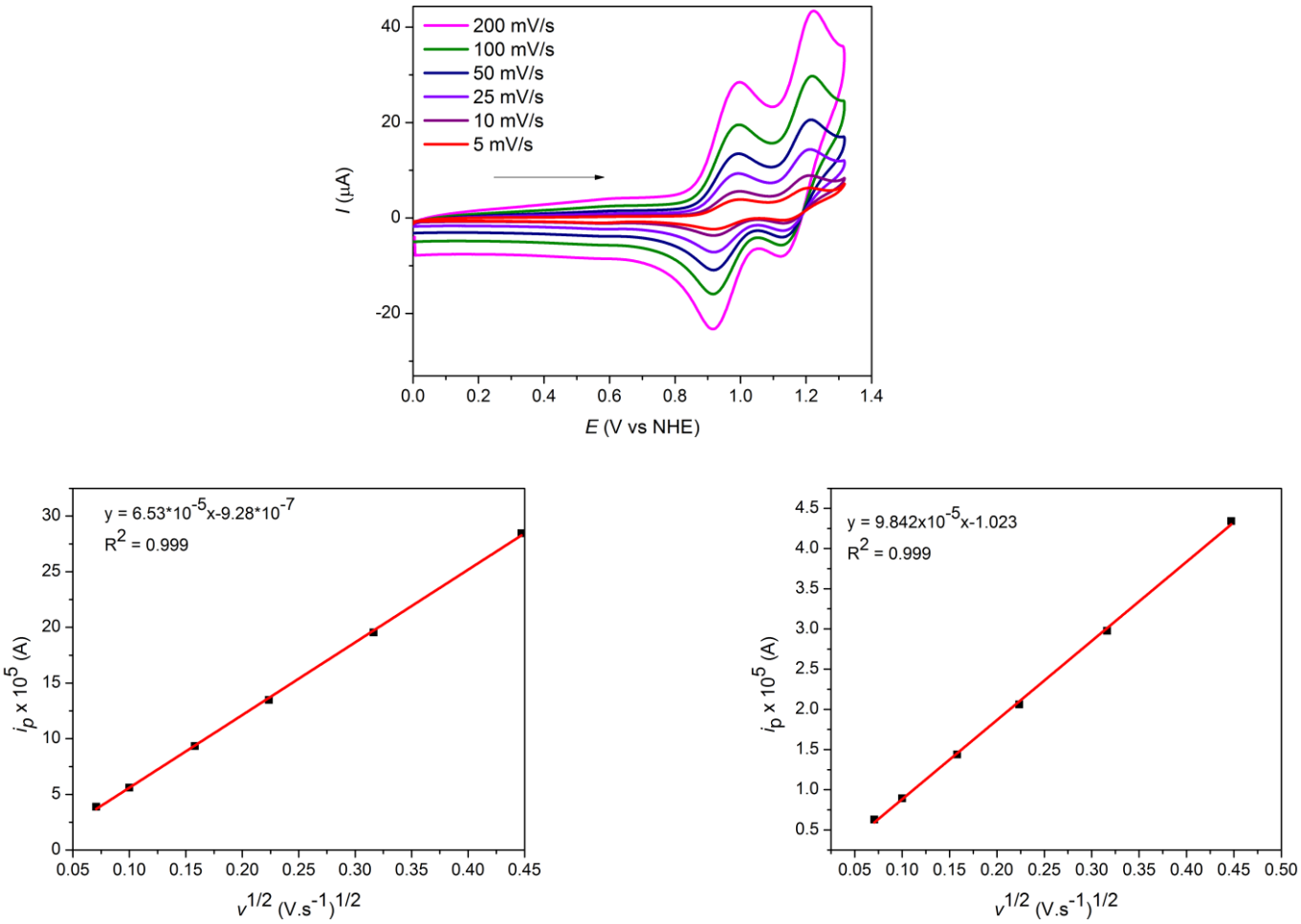

Fig. S14 Upper graph: CV of **[RuRu(py)$_4$Ru]** in 0.1 M triflic acid (pH = 1) at different scan rates. Lower graphs: Plots of the anodic current i_p ($Ru^{III/II}$) *vs* square root of the scan rate ($v^{1/2}$) for the first oxidation (left) and the second oxidation (right) process. Conditions: WE (glassy carbon electrode), CE (platinum wire), RE (Ag/AgCl 3M NaCl) and [C] = 1.28 mM.

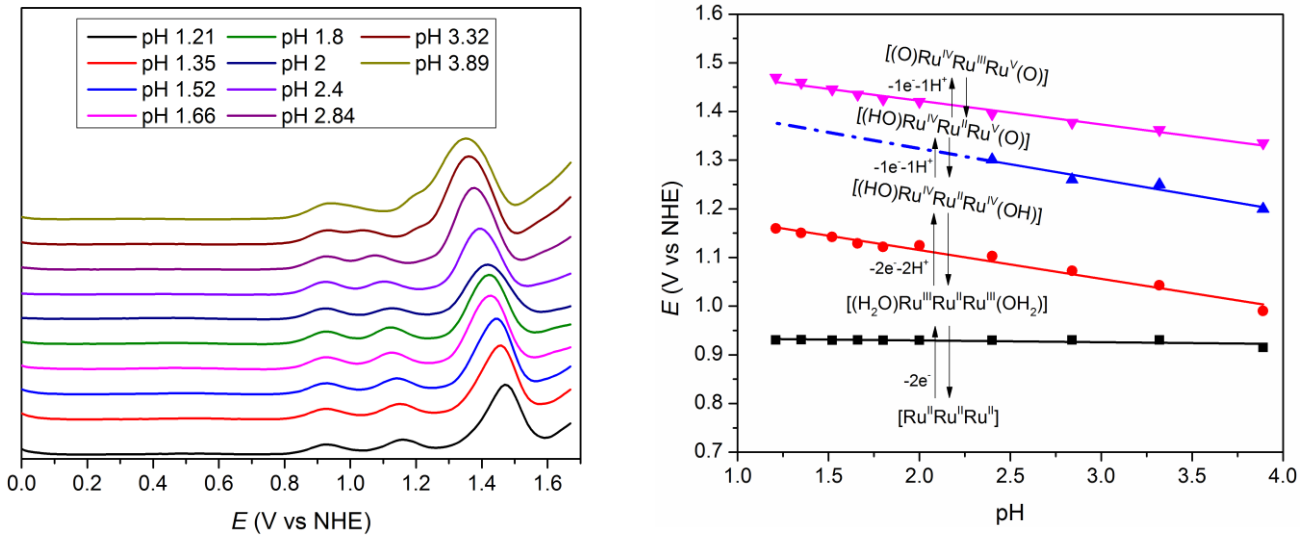

Fig. S15 SWV of **[RuRu(py)$_4$Ru]** at different pH´s (left). Potential vs pH diagram (right). Conditions: WE (glassy carbon electrode), CE (platinum wire), RE (Ag/AgCl 3M NaCl). v = 100 mV/s.

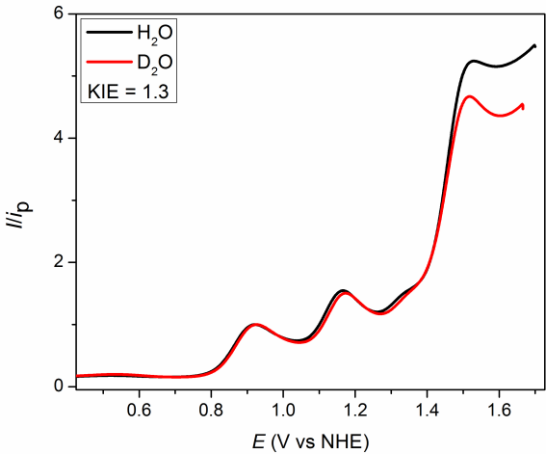

Fig. S16 Anodic scan of the CVs for **[RuRu(py)$_4$Ru]** in H_2O and D_2O at in 0.1 M triflic acid (pH = 1 and pD = 1). **[RuRu(py)$_4$Ru]** = 1.20 mM.

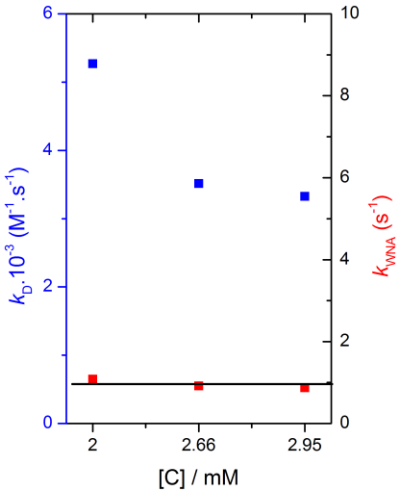

Fig. S17 Plot of calculated the k_{WNA} and k_D vs complex concentration [**RuRu(py)$_4$Ru**].

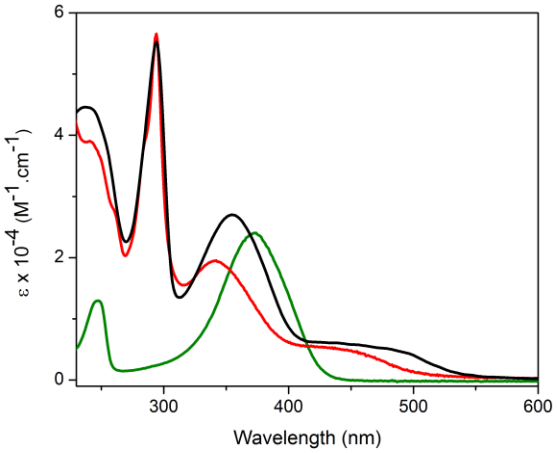

Fig. S18 UV-visible spectra of complexes ***trans*-Ru(tbupy)$_4$(CN)$_2$** (olive trace) and **[RuRu(tbupy)$_4$Ru]** (black trace) in CH_2Cl_2 and **[RuRu(py)$_4$Ru]** (red trace) in 0.1 M triflic acid (pH = 1) at 298 K.

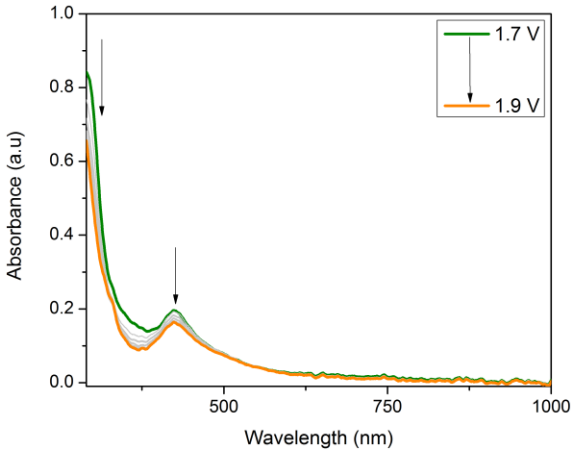

Fig. S19 UV-Vis spectroelectrochemistry for **[RuRu(tbupy)$_4$Ru]** in CH_2Cl_2 (0.2 M TBAH). The arrows indicate observed changes. Conditions: WE (platinum), CE (platinum), RE (Ag/AgCl 3M NaCl).

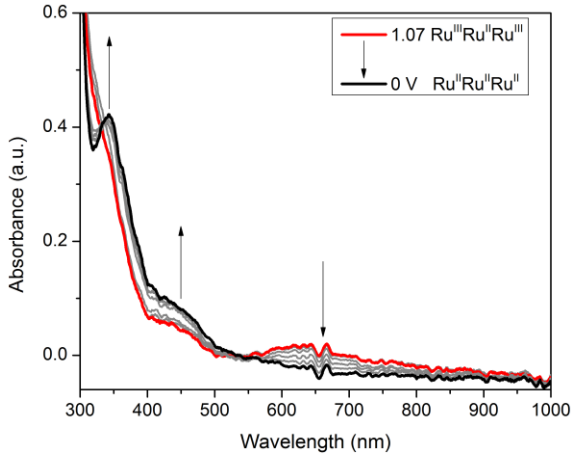

Fig. S20 UV-Vis spectroelectrochemistry of **[RuRu(py)$_4$Ru]** in 0.1 M triflic acid (pH = 1). The arrows indicate changes during the reduction process. Conditions: WE (platinum), CE (platinum), RE (Ag/AgCl 3M NaCl).

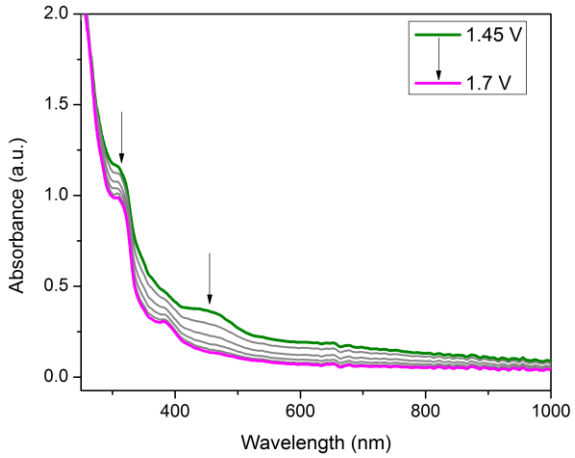

Fig. S21 UV-Vis spectroelectrochemistry of **[RuRu(py)$_4$Ru]** in 0.1 M triflic acid (pH = 1). The arrows indicate observed changes. Conditions: WE (platinum), CE (platinum), RE (Ag/AgCl 3M NaCl).

Table S1. Energies values and percentual group contributions of selected MOs of complex **[RuRu(tbupy)$_4$Ru]** in their singlet ground state.

MOs	Energy (eV)	Ru_{tbupy}	Ru_{bda}	tbupy	bda
L+10	-1.06	2	1	97	0
L+9	-1.23	5	0	95	0
L+8	-1.32	1	1	98	0
L+7	-1.37	4	0	96	0
L+6	-1.49	3	1	96	0
L+5	-1.87	0	4	0	96
L+4	-1.88	0	3	0	96
L+3	-2.16	0	2	0	98
L+2	-2.16	0	2	0	98
L+1	-2.55	0	7	0	92
LUMO	-2.55	1	7	0	92
HOMO	-5.35	25	54	2	20
H-1	-5.41	22	57	2	20
H-2	-5.48	31	50	2	17
H-3	-5.58	81	0	19	0
H-4	-5.59	33	48	3	17
H-5	-5.83	6	66	1	27
H-6	-5.96	7	66	1	26
H-7	-6.16	41	33	6	21
H-8	-6.25	36	39	6	19
H-9	-6.77	2	5	0	93
H-10	-6.78	1	5	0	94

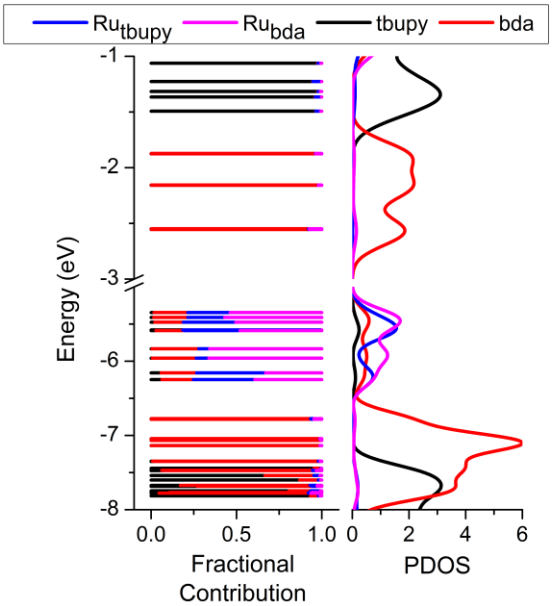

Fig. S22 Molecular orbital diagram and partial density of states (PDOS) of complex **[RuRu(tbupy)$_4$Ru]** in their singlet ground state.

Table S2. Energies values and percentual group contributions of selected alpha MOs of complex **[$Ru^{III}Ru^{II}(tbupy)_4Ru^{III}$]$^{2+}$** in their triplet ground state.

Alpha orbitals	Energy (eV)	Ru_{tbupy}	Ru_{bda}	tbupy	bda
L+10	-2.01	3	1	96	0
L+9	-2.66	9	59	0	32
L+8	-2.67	5	60	0	34
L+7	-2.69	1	62	0	37
L+6	-2.74	14	56	0	29
L+5	-3.02	0	2	0	98
L+4	-3.02	0	2	0	98
L+3	-3.23	0	1	0	98
L+2	-3.23	0	1	0	98
L+1	-3.72	0	4	0	95
LUMO	-3.72	0	4	0	95
HOMO	-6.28	81	0	19	0
H-1	-6.49	85	5	9	1
H-2	-6.5	85	4	9	1
H-3	-7.55	3	6	1	90
H-4	-7.56	2	8	0	90
H-5	-7.68	6	50	2	42
H-6	-7.71	6	45	6	43
H-7	-7.74	3	46	1	51
H-8	-7.75	3	46	1	50
H-9	-7.86	0	2	0	98
H-10	-7.86	0	2	1	97

Table S3. Energies values and percentual group contributions of selected beta MOs of complex **[Ru^{III}Ru^{II}(tbupy)$_4$Ru^{III}]$^{2+}$** in their triplet ground state.

Beta orbitals	eV	Ru_{tbupy}	Ru_{bda}	tbupy	bda
L+10	-2.83	2	4	92	2
L+9	-2.89	18	54	3	25
L+8	-3.29	0	2	0	97
L+7	-3.29	0	2	0	97
L+6	-3.5	0	1	0	99
L+5	-3.5	0	1	0	99
L+4	-3.98	0	4	0	96
L+3	-3.98	0	4	0	96
L+2	-4.94	1	72	0	27
L+1	-4.95	1	72	0	27
LUMO	-5.88	79	0	21	0
HOMO	-7.73	13	53	1	34
H-1	-7.81	7	49	1	44
H-2	-7.84	3	13	0	85
H-3	-7.85	2	6	0	92
H-4	-8.03	25	46	3	27
H-5	-8.11	1	3	0	96
H-6	-8.12	1	2	0	97
H-7	-8.19	8	55	2	34
H-8	-8.49	51	5	32	12
H-9	-8.57	35	12	39	14
H-10	-8.68	0	1	1	98

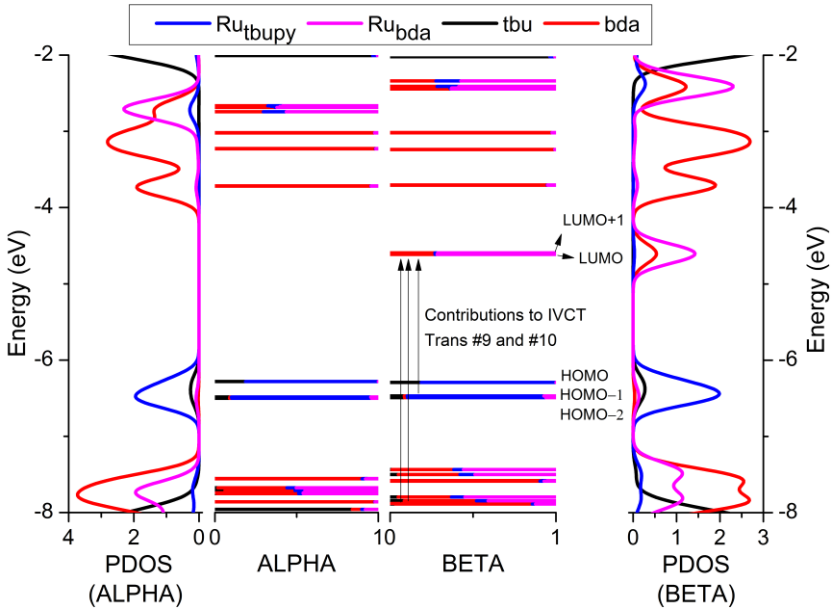

Fig. S23 Molecular orbital diagram and partial density of states (PDOS) of complex **[Ru^{III}Ru^{II}(tbupy)$_4$Ru^{III}]$^{2+}$** in their triplet ground state.

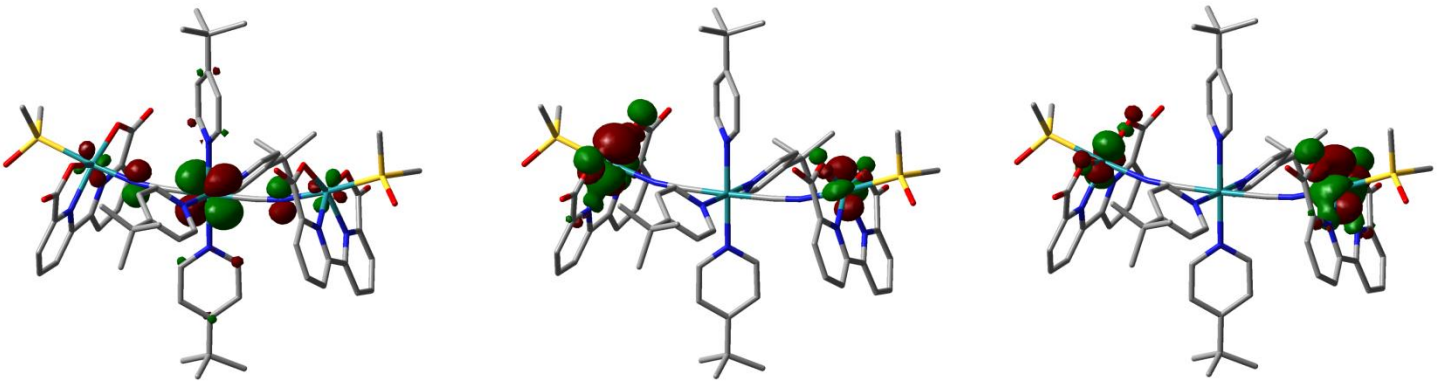

HOMO-2β
-6.48 eV

LUMO+1α
-4.58 eV

LUMO+2α
-3.69 eV

Fig. S24 Molecular orbitals of complex **[$Ru^{III}Ru^{II}(tbupy)_4Ru^{III}$]$^{2+}$** involved in MM´CT transitions.

Table S4. Energies values and percentual group contributions of selected alpha MOs of complex **[$Ru^{III}Ru^{III}(tbupy)_4Ru^{III}$]$^{3+}$** in their quartet ground state.

Alpha orbitals	eV	Ru_{tbupy}	Ru_{bda}	tbupy	bda
L+10	-2.87	2	1	97	0
L+9	-3.03	0	61	0	38
L+8	-3.05	0	61	0	39
L+7	-3.11	13	56	0	30
L+6	-3.25	17	49	2	32
L+5	-3.31	0	3	0	96
L+4	-3.32	1	5	0	95
L+3	-3.5	0	2	0	98
L+2	-3.51	1	3	0	96
L+1	-4	0	4	0	96
LUMO	-4	0	4	0	96
HOMO	-7.82	2	8	0	90
H-1	-7.83	2	8	0	90
H-2	-8	10	48	1	42
H-3	-8.05	4	44	1	52
H-4	-8.08	4	41	0	55
H-5	-8.1	2	36	0	62
H-6	-8.12	1	8	0	91
H-7	-8.13	1	15	0	84
H-8	-8.33	21	49	3	27
H-9	-8.44	8	53	4	35
H-10	-8.69	8	1	16	75

Table S5. Energies values and percentual group contributions of selected beta MOs of complex **[Ru^{III}Ru^{III}(tbupy)$_4$Ru^{III}]$^{3+}$** in their quartet ground state.

Beta orbitals	eV	Ru_{tbupy}	Ru_{bda}	tbupy	bda
L+10	-2.83	2	4	92	2
L+9	-2.89	18	54	3	25
L+8	-3.29	0	2	0	97
L+7	-3.29	0	2	0	97
L+6	-3.5	0	1	0	99
L+5	-3.5	0	1	0	99
L+4	-3.98	0	4	0	96
L+3	-3.98	0	4	0	96
L+2	-4.94	1	72	0	27
L+1	-4.95	1	72	0	27
LUMO	-5.88	79	0	21	0
HOMO	-7.73	13	53	1	34
H-1	-7.81	7	49	1	44
H-2	-7.84	3	13	0	85
H-3	-7.85	2	6	0	92
H-4	-8.03	25	46	3	27
H-5	-8.11	1	3	0	96
H-6	-8.12	1	2	0	97
H-7	-8.19	8	55	2	34
H-8	-8.49	51	5	32	12
H-9	-8.57	35	12	39	14
H-10	-8.68	0	1	1	98

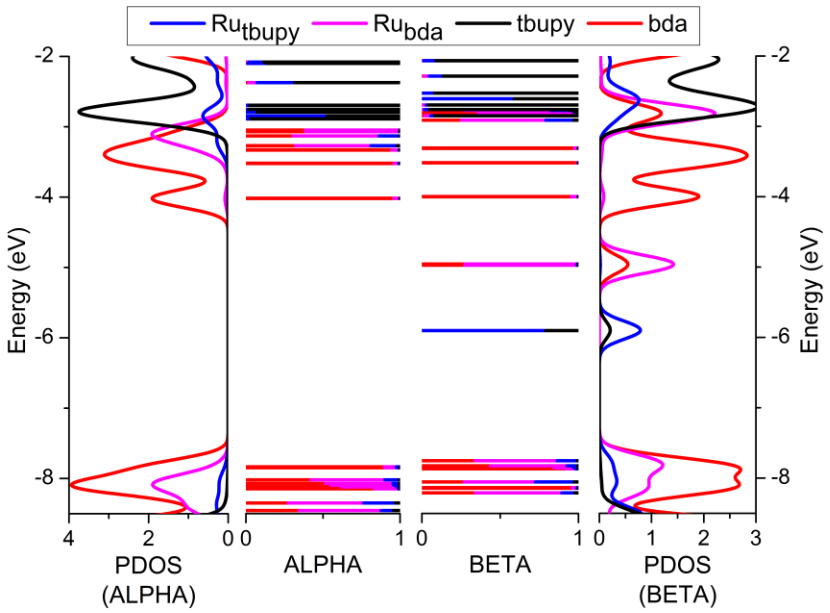

Fig. S25 Molecular orbital diagram and partial density of states (PDOS) of complex **[Ru^{III}Ru^{III}(tbupy)$_4$Ru^{III}]$^{3+}$** in their quartet ground state.

Table S6. (TD)DFT assignments for calculated UV-Vis transitions of complex **[RuRu(tbupy)$_4$Ru]** in their singlet ground state.

No.	Wavelength (nm)	Osc. Strength	Major contributions	Assignment
6	516.7	0.0184	H-4->L+1 (14%) H-1->L+2 (14%) HOMO->L+1 (27%) HOMO->L+3 (19%)	d(Ru_{bda},Ru_{tbupy})->π*(bda)
8	506.4	0.0108	H-4->L+1 (17%) H-1->L+2 (16%) HOMO->L+1 (10%) HOMO->L+3 (24%)	d(Ru_{bda},Ru_{tbupy})->π*(bda)
16	456.0	0.0203	H-5->LUMO (12%) H-2->LUMO (11%) H-2->L+3 (12%) H-1->L+3 (10%)	d(Ru_{bda}) -> π*(bda)
32	406.1	0.0255	H-4->L+5 (30%) HOMO->L+5 (19%)	d(Ru_{bda},Ru_{tbupy})->π*(bda)
34	398.1	0.0338	H-6->LUMO (10%) H-2->L+5 (29%) H-1->L+5 (32%)	d(Ru_{bda},Ru_{tbupy})>π*(bda,tbupy)
51	370.0	0.0432	H-3->L+6 (37%) HOMO->L+6 (17%)	d(Ru_{tbupy}) ->π*(tbupy) d(Ru_{bda}) ->π*(bda)
53	368.4	0.0702	H-6->L+2 (11%) H-3->L+6 (12%) HOMO->L+7 (21%)	d(Ru_{tbupy}) ->π*(tbupy) d(Ru_{bda}) ->π*(bda)
59	354.8	0.0635	H-3->L+7 (15%) H-2->L+8 (21%) H-1->L+8 (29%)	d(Ru_{bda},Ru_{tbupy})->π*(tbupy)
63	352.0	0.1255	H-3->L+8 (36%)	d(Ru_{bda},Ru_{tbupy})->π*(tbupy)
64	351.6	0.1467	H-3->L+7 (11%) H-3->L+8 (16%) H-2->L+9 (12%) H-1->L+9 (15%)	d(Ru_{bda},Ru_{tbupy})->π*(tbupy)
69	346.2	0.0995	H-4->L+6 (57%) HOMO->L+6 (11%)	d(Ru_{bda},Ru_{tbupy})->π*(tbupy)
141	291.3	0.0693	H-21->LUMO (10%) H-18->LUMO (12%)	d(Ru_{bda},Ru_{tbupy})->π*(tbupy)
166	282.9	0.1026	H-8->L+8 (27%) H-4->L+15 (17%) HOMO->L+15 (14%)	d(Ru_{bda},Ru_{tbupy})>π*(bda,tbupy) π(bda)>π*(bda)

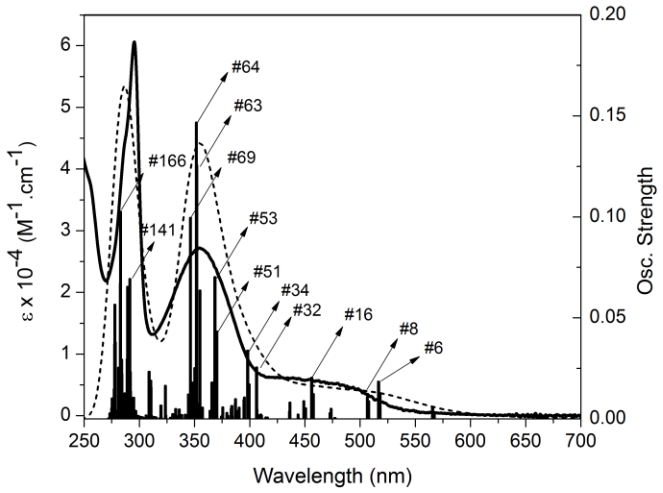

Fig. S26 (TD)DFT-calculated (dashed curve) and experimental (solid curve) UV-visible absorption spectra of complex **[RuRu(tbupy)$_4$Ru]** in their singlet ground state. Calculated transition are represented by black vertical bars.

Table S7. (TD)-DFT assignments for calculated UV-Vis transitions of complex **[Ru^{III}Ru^{II}(tbupy)$_4$Ru^{III}]$^{2+}$** in their triplet ground state.

No.	Wavelength (nm)	Osc. Strength	Major contributions	Assignment
9	817.7	0.0114	H-8β->LUMOβ (13%) H-7β ->LUMOβ (10%) H-2β->LUMOβ (53%)	d(Ru$_{tbupy}$) ->d(Ru$_{bda}$)
10	811.9	0.0053	H-8β->L+1β (12%), H-7β->L+1β (11%) H-2β->L+1β (52%)	d(Ru$_{tbupy}$) ->d(Ru$_{bda}$)
23	536.3	0.0075	H-2α ->LUMOα (49%) H-2β->L+2β (39%)	d(Ru$_{tbupy}$) ->π*(bda)
24	535.2	0.0038	H-2α->L+1α (48%) H-2β->L+3β (40%)	d(Ru$_{tbupy}$) ->π*(bda)
102	391.7	0.0122	H-6β->L+2β (21%) H-5β->L+3β (27%)	d(Ru$_{tbupy}$) ->π*(bda)
140	355.5	0.0459	HOMO α->L+10α (38%) HOMO β->L+12β (42%)	d(Ru$_{tbupy}$) ->π*(tbupy)
159	345.9	0.0521	H-1α->L+28α (11%) HOMO α->L+11α (23%) HOMO β->L+13β (28%)	d(Ru$_{tbupy}$) ->π*(tbupy)
160	345.8	0.0417	H-1α->L+28α (15%) HOMO α->L+11α (20%) HOMO β->L+13β (17%)	d(Ru$_{tbupy}$) ->π*(tbupy)
189	334.7	0.0799	H-2α->L+10α (13%) HOMO α->L+13α (28%) H-2β->L+12β (12%) HOMO β->L+15β (29%)	d(Ru$_{tbupy}$) ->π*(tbupy)
218	322.1	0.1031	H-1α->L+13α (42%) H-1β->L+14β (32%)	d(Ru$_{tbupy}$) ->π*(tbupy)
321	290.9	0.2091	HOMO β->L+16β (13%)	d(Ru$_{tbupy}$) ->π*(bda)

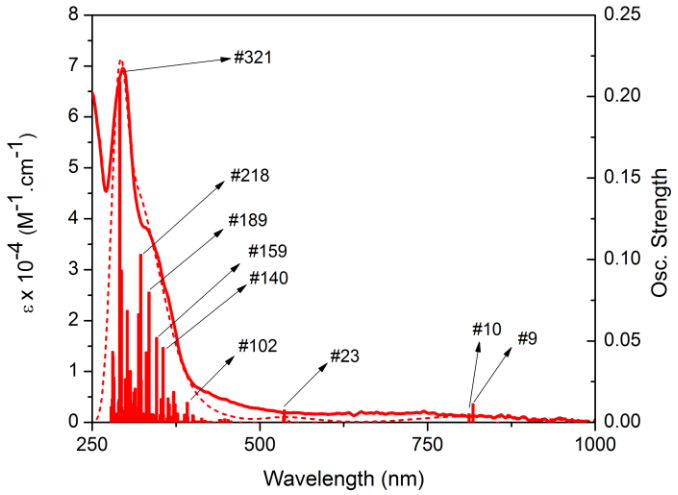

Fig. S27 Left: (TD)DFT-calculated (dashed curve) and experimental (solid curve) UV-visible absorption spectra of complex **[$Ru^{III}Ru^{II}(tbupy)_4Ru^{III}$]$^{2+}$** in their triplet ground state. Calculated transition are represented by red vertical bars.

Table S8. (TD)DFT assignments for calculated UV-Vis transitions of complex **[$Ru^{III}Ru^{III}(tbupy)_4Ru^{III}$]$^{3+}$** in their quartet ground state.

No.	Wavelength (nm)	Osc. Strength	Major contributions	Assignment
12	676.3	0.0033	H-9 β ->LUMO β (43%) H-4 β ->LUMO β (51%)	d(Ru_{tbupy}),π(bda)->d(Ru_{tbupy})
23	521.8	0.0066	H-20 β ->LUMO β (82%)	π (tbupy)->d(Ru_{tbupy})
34	481.8	0.083	H-22 β ->LUMO β (83%)	π(tbupy)->d(Ru_{tbupy})
35	478.7	0.0733	H-21 β ->LUMO β (75%)	π(tbupy)->d(Ru_{tbupy})
94	373.9	0.043	H-26 β ->L+2 β (40%) H-14 β ->L+2 β (19%)	π(tbupy,bda)->d(Ru_{tbupy})
97	370.0	0.0117	H-26 β ->L+2 β (11%) H-14 β ->L+2 β (67%)	π(tbupy) ->d(Ru_{bda})
257	291.2	0.0804	H-12 α ->L+1 α (13%) H-2 α ->L+3 α (12%) H-4 β ->L+8 β (10%)	d(Ru_{bda}) ->π*(bda)
269	288.1	0.0869	H-3 β ->L+13 β (10%) H-2 β ->L+9 β (16%)	π(bda) -> d(Ru_{bda})

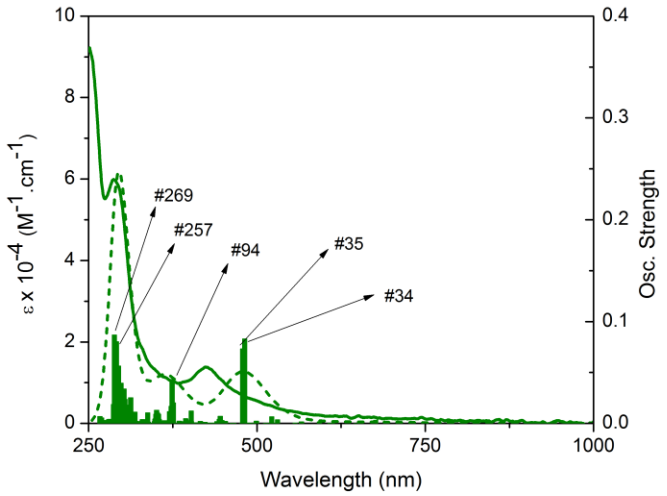

Fig. S28 (TD)DFT-calculated (dashed curve) and experimental (solid curve) UV-visible absorption spectra of complex **[$Ru^{III}Ru^{III}$(tbupy)$_4Ru^{III}$]$^{3+}$** in their quartet ground state. Calculated transition are represented by green vertical bars.

Table S9. Energies values and percentual group contributions of selected MOs of complex **[$Ru^{II}Ru^{II}$(py)$_4Ru^{II}$]** in their singlet ground state.

MO´s	Energy (eV)	Ru_{py}	Ru_{bda}	py	bda
L+10	-1.2	1	1	98	0
L+9	-1.5	6	0	94	0
L+8	-1.6	2	1	97	0
L+7	-1.61	3	0	96	1
L+6	-1.63	2	1	97	0
L+5	-1.93	0	4	0	96
L+4	-1.94	0	3	0	96
L+3	-2.2	0	1	0	98
L+2	-2.21	0	1	0	98
L+1	-2.57	0	7	0	92
LUMO	-2.58	0	7	0	92
HOMO	-5.48	19	59	1	21
H-1	-5.54	10	67	1	23
H-2	-5.61	37	47	2	14
H-3	-5.73	32	49	2	16
H-4	-5.81	83	0	17	0
H-5	-5.94	6	67	1	27
H-6	-6.05	7	68	0	25
H-7	-6.31	48	28	6	18
H-8	-6.39	43	34	6	17
H-9	-6.91	2	5	0	93
H-10	-6.92	2	5	0	94

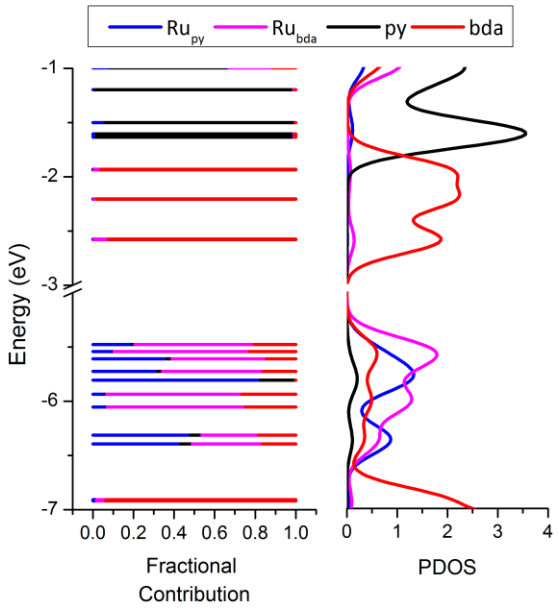

Fig. S29 Molecular orbital diagram and partial density of states (PDOS) of complex **[Ru^{II}Ru^{II}(py)$_4$Ru^{II}]** in their singlet ground state.

Table S10. Energies values and percentual group contributions of selected alpha MOs of the complex **[Ru^{III}Ru^{II}(py)$_4$Ru^{III}]$^{2+}$** in their triplet ground state.

MOs	Energy (eV)	Ru_{py}	Ru_{bda}	py	bda	H_2O
L+10	-1.74	2	1	97	0	0
L+9	-2.23	15	57	0	27	1
L+8	-2.3	14	57	0	28	1
L+7	-2.49	0	56	0	44	0
L+6	-2.5	0	54	0	46	0
L+5	-2.56	0	10	0	90	0
L+4	-2.57	0	12	0	88	0
L+3	-2.73	0	1	0	98	0
L+2	-2.74	0	2	0	98	0
L+1	-3.24	0	4	0	96	0
LUMO	-3.24	0	4	0	96	0
HOMO	-6.02	83	0	17	0	0
H-1	-6.18	86	5	8	1	0
H-2	-6.18	87	5	7	1	0
H-3	-6.84	0	46	0	43	10
H-4	-6.84	0	46	0	43	10
H-5	-7.22	3	7	0	89	0
H-6	-7.23	3	8	0	89	0
H-7	-7.32	5	50	1	43	0
H-8	-7.37	6	44	3	47	0
H-9	-7.51	0	3	0	97	0
H-10	-7.52	0	3	0	96	0

Table S11. Energies values and percentual group contributions of selected beta MOs of the complex **[$Ru^{III}Ru^{II}(py)_4Ru^{III}$]$^{2+}$** in their triplet ground state.

MOs	Energy (eV)	Ru_{py}	Ru_{bda}	py	bda	H_2O
L+10	-1.94	14	59	0	26	1
L+9	-2.24	0	64	0	36	0
L+8	-2.26	0	64	0	36	0
L+7	-2.54	0	3	0	97	0
L+6	-2.55	0	3	0	97	0
L+5	-2.73	0	1	0	99	0
L+4	-2.73	0	1	0	99	0
L+3	-3.2	0	8	0	92	0
L+2	-3.21	0	8	0	92	0
L+1	-3.74	0	68	0	26	6
LUMO	-3.74	0	68	0	26	6
HOMO	-6.02	83	0	17	0	0
H-1	-6.15	84	7	7	2	0
H-2	-6.15	83	8	7	2	0
H-3	-7.07	5	58	1	36	0
H-4	-7.14	9	50	3	38	0
H-5	-7.2	4	18	1	77	0
H-6	-7.21	4	9	1	86	0
H-7	-7.36	8	51	2	38	1
H-8	-7.44	12	54	5	29	1
H-9	-7.51	0	1	0	99	0
H-10	-7.51	0	1	0	99	0

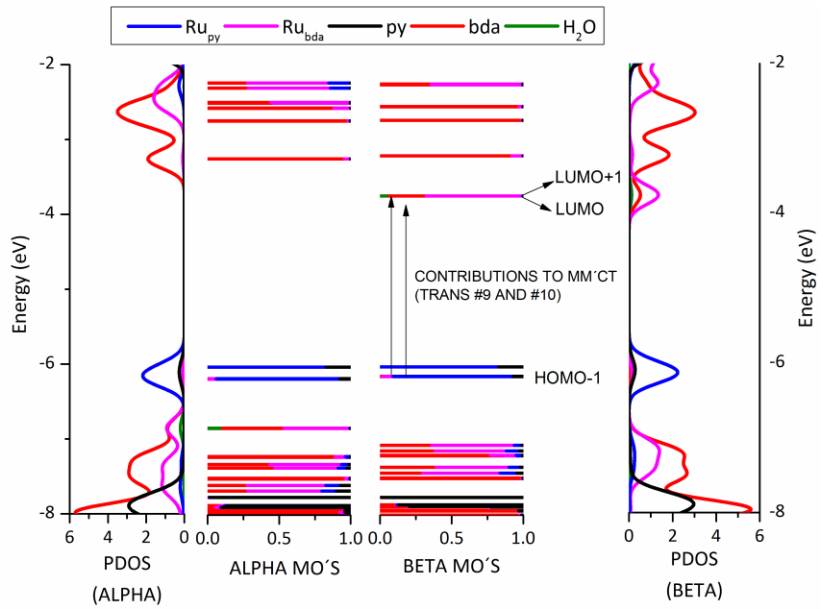

Fig. S30 Molecular orbital diagram and partial density of states (PDOS) of complex **[$Ru^{III}Ru^{II}(py)_4Ru^{III}$]$^{2+}$** in their triplet ground state.

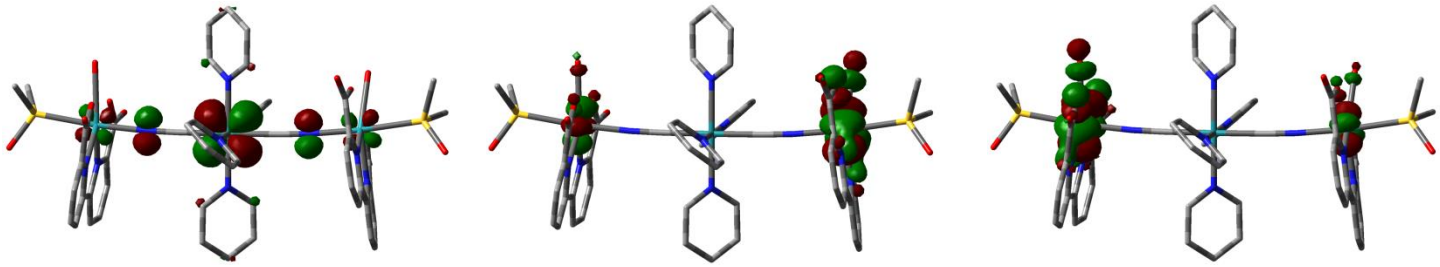

HOMO-2β
-6.15 eV

LUMO β
-3.74 eV

LUMO+1β
-3.74 eV

Fig. S31 Molecular orbitals of complex **[$Ru^{III}Ru^{II}(py)_4Ru^{III}$]$^{2+}$** involved in MM´CT transitions #9 and #10.

Table S12. Energies values and percentual group contributions of selected alpha MOs of the complex **[$Ru^{V}Ru^{II}(py)_4Ru^{IV}$]$^{2+}$** in their doublet ground state.

MOs	Energy (eV)	Ru_{py}	Ru_{bdaOH}	Ru_{bdaO}	py	bda_{OH}	bda_{O}	OH	O
L+10	-2.66	10	1	49	0	0	23	0	17
L+9	-2.71	0	0	1	0	2	97	0	0
L+8	-2.72	0	1	0	0	97	2	0	0
L+7	-2.86	0	0	2	0	0	97	0	1
L+6	-2.87	0	1	0	0	99	0	0	0
L+5	-3.41	0	0	4	0	0	95	0	1
L+4	-3.43	0	5	0	0	95	0	0	0
L+3	-3.57	1	55	0	0	31	0	13	0
L+2	-3.79	6	0	54	0	0	35	0	5
L+1	-3.9	0	60	0	0	32	0	8	0
LUMO	-4.39	0	0	56	0	0	31	0	13
HOMO	-6.16	83	0	0	17	0	0	0	0
H-1	-6.38	88	2	1	8	0	0	0	0
H-2	-6.4	88	2	1	9	0	0	0	0
H-3	-7.33	3	5	0	0	91	0	1	0
H-4	-7.49	3	0	6	0	0	88	0	2
H-5	-7.61	1	5	0	0	94	0	0	0
H-6	-7.7	3	31	0	3	53	0	9	0
H-7	-7.78	1	6	0	1	63	0	28	0
H-8	-7.79	0	0	1	7	0	92	0	0
H-9	-7.8	0	1	0	90	1	8	0	0
H-10	-7.87	4	8	3	76	2	6	1	0

Table S13. Energies values and percentual group contributions of selected beta MOs of the complex **[$Ru^{V}Ru^{II}(py)_4Ru^{IV}$]$^{2+}$** in their doublet ground state.

MOs	Energy (eV)	Ru_{py}	Ru_{bdaOH}	Ru_{bdaO}	py	bda_{OH}	bda_{O}	OH	O
L+10	-2.71	0	0	1	0	2	97	0	0
L+9	-2.72	0	1	0	0	97	2	0	0
L+8	-2.85	0	0	1	0	0	98	0	1
L+7	-2.87	0	1	0	0	99	0	0	0
L+6	-3.29	0	0	6	0	0	88	0	6
L+5	-3.43	0	5	0	0	95	0	0	0
L+4	-3.57	1	52	4	0	29	2	12	1
L+3	-3.59	6	4	53	0	2	28	1	7
L+2	-3.9	0	60	0	0	32	0	8	0
L+1	-4.17	0	0	54	0	0	24	0	21
LUMO	-4.68	2	0	30	0	0	16	0	51
HOMO	-6.15	83	0	0	17	0	0	0	0
H-1	-6.38	88	2	1	8	0	0	0	0
H-2	-6.38	87	2	0	8	0	1	0	1
H-3	-7.33	3	5	0	0	91	0	1	0
H-4	-7.51	3	0	7	0	0	90	0	0
H-5	-7.61	1	5	0	0	94	0	0	0
H-6	-7.7	3	31	0	3	53	0	9	0
H-7	-7.76	0	0	0	1	0	76	0	22
H-8	-7.78	1	6	0	2	61	3	28	0
H-9	-7.79	0	0	1	4	2	91	1	0
H-10	-7.8	0	1	0	92	1	6	0	0

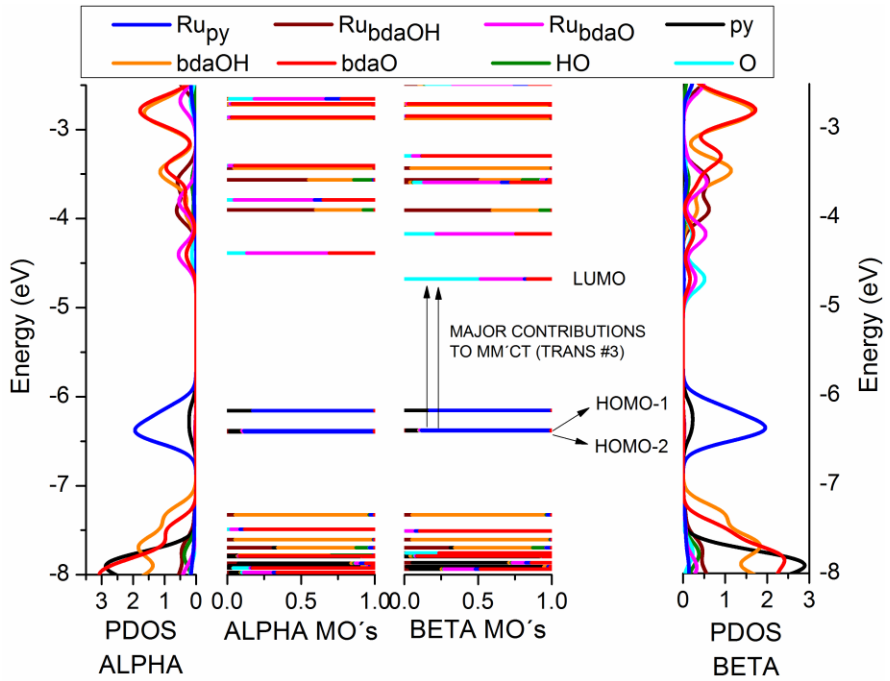

Fig. S32 Molecular orbital diagram and partial density of states (PDOS) of complex **[$Ru^{V}Ru^{II}(py)_4Ru^{IV}$]$^{2+}$** in their doublet ground state.

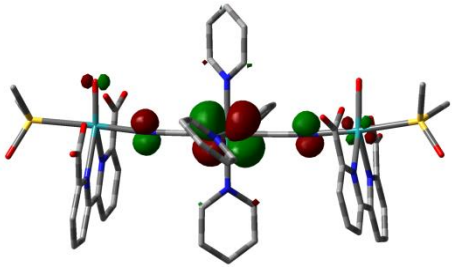

HOMO-2β
-6.38 eV

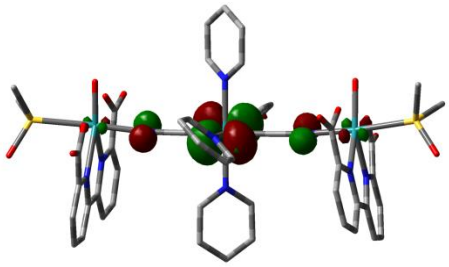

HOMO-1β
-6.38 eV

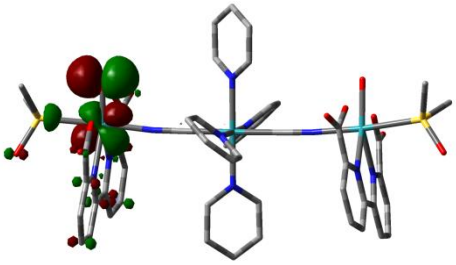

LUMO β
-4.68 eV

Fig. S33 Molecular orbitals of complex **[$Ru^{V}Ru^{II}(py)_4Ru^{IV}$]$^{2+}$** involved in MM´CT transitions #3.

Table S14. (TD)DFT assignments for calculated UV-Vis transitions of complex **[$Ru^{II}Ru^{II}(py)_4Ru^{II}$]** in their singlet ground state.

No.	Wavelength (nm)	Osc. Strength	Major contributions	Assignment
6	498.3	0.0151	H-3->L+1 (10%) H-1->L+2 (22%) HOMO->L+1 (18%) HOMO->L+3 (24%)	d(Ru_{bda},Ru_{py})->π*(bda)
8	489.7	0.0193	H-3->L+1 (27%) H-1->L+2 (10%) HOMO->L+1 (14%) HOMO->L+3 (16%)	d(Ru_{bda},Ru_{py})->π*(bda)
16	442.0	0.0316	H-5->L+2 (13%) H-2->L+2 (23%) H-2->L+3 (17%)	d(Ru_{bda},Ru_{py})->π*(bda)
36	389.1	0.0292	H-2->L+5 (46%) H-1->L+5 (16%)	d(Ru_{bda},Ru_{py})->π*(bda)
60	360.2	0.1275	H-4->L+4 (10%) H-4->L+7 (13%) H-4->L+8 (41%) HOMO->L+9 (11%)	d(Ru_{py},Ru_{bda}) ->π*(py)
61	357.3	0.0839	H-4->L+5 (10%) H-4->L+7 (28%) H-4->L+8 (10%) H-1->L+6 (22%)	d(Ru_{py},Ru_{bda}) ->π*(py)
69	346.3	0.0474	H-5->L+4 (20%) H-5->L+5 (29%)	d(Ru_{bda},Ru_{py})->π*(bda)
71	342.3	0.0119	H-6->L+5 (39%) H-3->L+4 (10%)	d(Ru_{bda},Ru_{py})->π*(bda)
105	310.7	0.0376	H-2->L+11 (17%) H-2->L+12 (10%) H-2->L+13 (12%) H-1->L+11 (12%)	d(Ru_{py},Ru_{bda}) ->π*(py)
147	286.6	0.2903	H-18->LUMO (13%) H-18->L+1 (11%) H-17->LUMO (11%) H-17->L+1 (12%) H-10->L+4 (13%) H-9->L+5 (20%)	π(bda)>π*(bda)
148	285.2	0.0875	H-17->L+1 (12%) H-10->L+5 (14%) H-9->L+4 (26%) H-9->L+5 (25%)	π(bda)>π*(bda)
266	247.0	0.1809	H-2->L+18 (22%) H-2->L+20 (10%)	d(Ru_{py},Ru_{bda})->π*(bda)

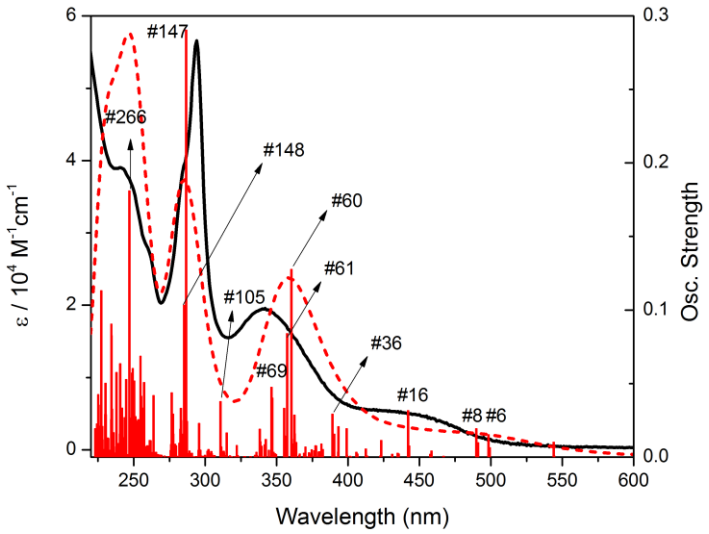

Fig. S34 (TD)DFT-calculated (dashed curve) and experimental (solid curve) UV-visible absorption spectra of complex **[Ru^{II}Ru^{II}(py)$_4$Ru^{II}]** in their singlet ground state. Calculated transition are represented by red vertical bars.

Table S15. (TD)DFT assignments for calculated UV-Vis transitions of the complex **[Ru^{III}Ru^{II}(py)$_4$Ru^{III}]$^{2+}$** in their triplet ground state.

No.	Wavelength (nm)	Osc. Strength	Major contributions	Assignment
9	604.0	0.0009	H-8 β ->LUMO β(15%) H-1 β ->LUMO β(61%)	d(Ru$_{py}$) -> d(Ru$_{bda}$)
10	603.8	0.0003	H-8 β ->L+1 β(13%) H-1 β ->L+1 β(54%)	d(Ru$_{py}$) -> d(Ru$_{bda}$)
11	582.2	0.0056	H-4 α->L+4 α (13%) H-4 α->L+6 α (62%) H-3 α->L+6 α (11%)	d(Ru$_{bda}$) -> d(Ru$_{bda}$)
12	579.5	0.0059	H-4 α->L+7 α (12%) H-3 α->L+5 α (10%) H-3 α->L+7 α (65%)	d(Ru$_{bda}$) -> d(Ru$_{bda}$)
28	504.6	0.005	H-1 α->L+1 α (36%) H-1 β ->L+3 β(33%)	d(Ru$_{py}$) -> π*(bda)
99	375.8	0.0159	H-6 α->LUMO α (14%) H-6 β ->L+2 β(31%) H-5 β ->L+2 β(13%)	LLCT (DMSO->bda)
123	357.6	0.0468	HOMO α->L+10 α (35%) HOMO β ->L+12 β(39%)	d(Ru$_{py}$) -> π*(py)
124	356.5	0.0444	HOMO α->L+11 α (36%) HOMO β ->L+13 β(39%)	d(Ru$_{py}$) -> π*(py)
180	334.2	0.1576	H-1 α->L+12 α (15%) H-1 α->L+13 α (14%) H-1 β ->L+14 β(12%) H-1 β ->L+15 β(14%)	d(Ru$_{py}$) -> π*(py)
182	333.0	0.1204	H-2 α->L+13 α (19%) H-2 β ->L+15 β(18%)	d(Ru$_{py}$) -> π*(py)
309	287.7	0.107	H-1 β ->L+19 β(12%)	d(Ru$_{py}$) -> π*(py)
380	273.3	0.1078	H-6 β ->L+10 β(23%) H-5 β ->L+11 β(14%)	LMCT (DMSO->Ru$_{bda}$) LLCT (DMSO->bda)

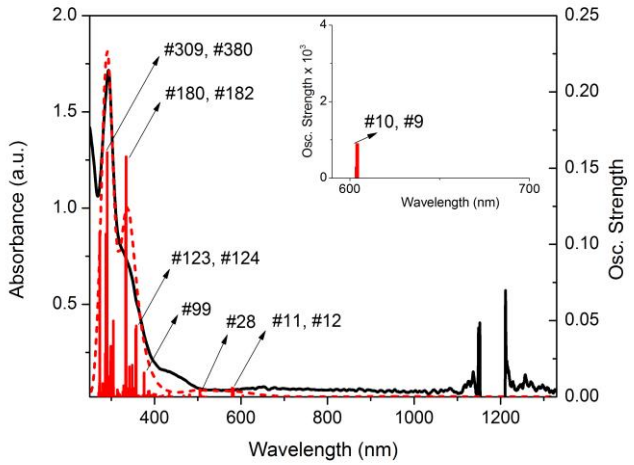

Fig. S35 (TD)DFT-calculated (dashed curve) and experimental (solid curve) UV-visible absorption spectra of complex **[Ru^{III}Ru^{II}(py)$_4$Ru^{III}]$^{2+}$** in their triplet ground state. Calculated transition are represented by red vertical bars.

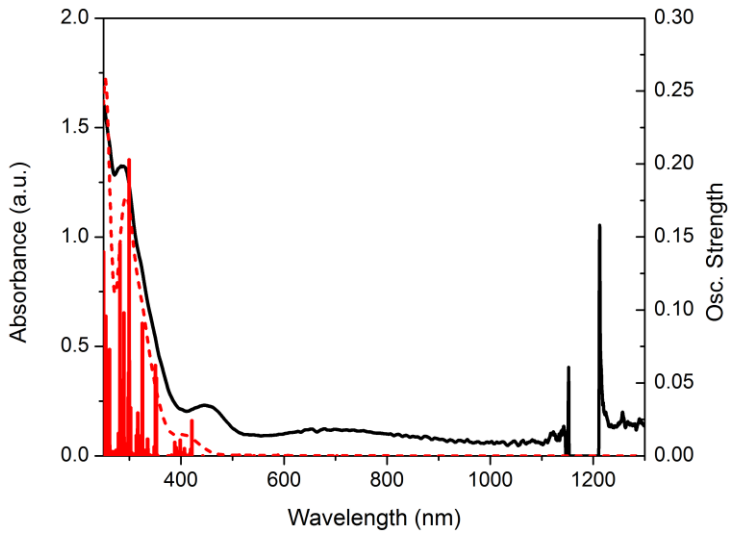

Fig. S36 Left: (TD)DFT-calculated (dashed curve) and experimental (solid curve) UV-visible absorption spectra of complex **[Ru^{IV}Ru^{II}(py)$_4$Ru^{IV}]$^{2+}$** in their singlet ground state. Calculated transition are represented by red vertical bars.

Table S16. (TD)DFT assignments for calculated UV-Vis transitions of the complex **[$Ru^{V}Ru^{II}(py)_4Ru^{IV}$]$^{2+}$** in their doublet ground state.

No.	Wavelength (nm)	Osc. Strength	Major contributions	Assignment
3	1092.7	0.0275	H-2β->LUMOβ (88%) H-1β->LUMOβ (10%)	d(Ru_{py}) -> d(Ru_{bdaO})
25	616.1	0.0078	H-4β->LUMOβ (91%)	π(bdaO) -> d(Ru_{bdaO})
125	397.2	0.0482	H-4α->L+2α (21%) H-4β->L+3β (48%)	π(bdaO) -> d(Ru_{bdaO})
210	348.4	0.0561	HOMOα->L+12α (41%) HOMOβ->L+13β (43%)	d(Ru_{py}) -> π*(py)
211	347.0	0.0623	HOMOα->L+13α (45%) HOMOβ->L+14β (46%)	d(Ru_{py}) -> π*(py)
307	320.5	0.0477	H-1α->L+15α (10%) H-4β->L+5β (11%)	d(Ru_{py}) -> π*(py)
308	320.2	0.0971	H-2α->L+14α (18%) H-29β->LUMOβ (20%) H-2β->L+15β (13%)	d(Ru_{py}) -> π*(py)

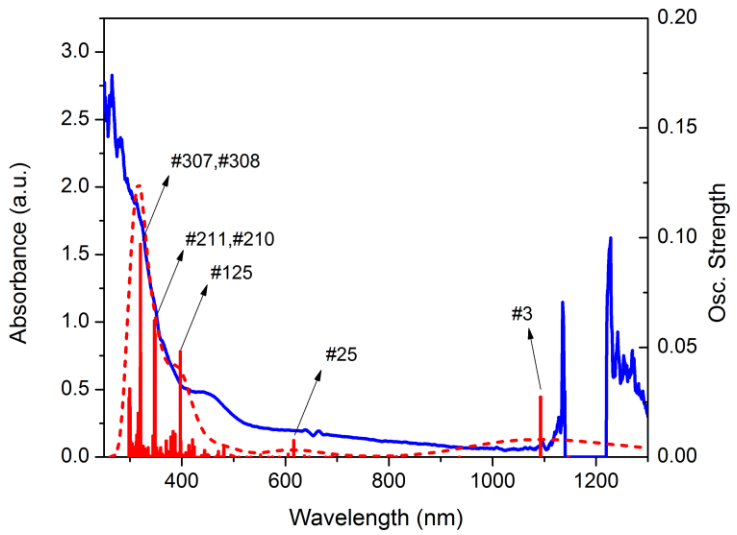

Fig. S37 Left: (TD)DFT-calculated (dashed curve) and experimental (solid curve) UV-visible absorption spectra of complex **[$Ru^{V}Ru^{II}(py)_4Ru^{IV}$]$^{2+}$** in their triplet ground state. Calculated transition are represented by red vertical bars.